NATIONAL TECHNICAL UNIVERSITY OF UKRAINE
“IGOR SIKORSKY KYIV POLYTECHNIC INSTITUTE”

Faculty of Physical Engineering

Department of High Temperature Materials and Powder Metallurgy

«On the rights of the manuscript»
УДК 621.793.79

«Admission to the defence»
Head of the department
__________ V.I. Mazur
«___»_____________2020

Master's thesis
for a master's degree
in the specialty 132 Materials Science
on the topic: «Oxidation resistance of cold-sprayed AlNiCoFeCrTi high-entropy coating »

Performed by
second-year student of group FN-81mn
Olajide Akinola Iyanu __________

Research supervisor:
professor of the department of HTM and PM, doctor of technical sciences, professor
Yurkova A.I.

Рецензент:
Професор кафедри фізики металів, д.т.н., професор
Макогон Ю.М. __________

I certify that in this master's dissertation there are no borrowings from the works of other authors without proper references.
Student _____________

Kyiv - 2020

NATIONAL TECHNICAL UNIVERSITY OF UKRAINE

“IGOR SIKORSKY KYIV POLYTECHNIC INSTITUTE”

Faculty of Physical Engineering

Department of High Temperature Materials and Powder Metallurgy

Education level	Second (master's)
Specialty	132 Materials science
Educational program	Nanotechnologies and computer design of materials

ЗАТВЕРДЖУЮ

Завідувач кафедри

__________ В.І. Мазур

«___»_____________2020 р

TASK

for the master's dissertation of the student

Olajide Akinola Iyanu

1. Topic of master's thesis: «Oxidation resistance of cold-sprayed AlNiCoFeCrTi high-entropy coating», Research supervisor: professor, doctor of technical science Yurkova Alexandra Ivanovna, approved by order of the University of «___»_________ 2020 р. No_____

2. The deadline for submission of the dissertation by a student is May 15, 2020

3. Object of the research is AlNiCoFeCrTi high-entropy cold-sprayed coating.

4. Subject of the research is high-temperature oxidation behavior of AlNiCoFeCrTi high-entropy coatings resulted from cold spray

5. List of tasks to be developed:

a) Literary review:

– to perform the analysis of contemporary world literary publications on the features of the structure and properties of high-entropy alloys and high-entropy coatings;

– to perform the analysis of the production methods of high-entropy powder alloys and their influence on the structure and properties;

– to analyze the production methods of coatings from high-entropy alloys, their capabilities and impact on the structure and properties of high-entropy coatings.

b) Experimental:

– Select and validate the chemical composition of high-entropy coatings;

– Study the structure and phase composition, size and hardness of the particles of feedstock powder;

- Obtain high-entropy coatings by cold gas-dynamic spraying;

– Investigate the structure, phase composition and microhardness of coatings obtained by the CS process.

– Carry out the oxidation of coatings at a temperature of 900 °C for 100 hours.

– Investigation of structure, phase, chemical composition and microhardness of coatings obtained by the CS process after high-temperature oxidation;

c) Discussion of the results:

– analyze the results and draw conclusions.

6. Approximate list of graphic (illustrative) material:

– topic of work, its actuality, purpose and main tasks;

– methods of obtaining high-entropy powder alloy and coatings from it;

– selection and validation of research material;

– research methods (characterization techniques) for structure, phase composition and microhardness of powder alloy and coatings before and after oxidation;

– experimental data on the structure and phase composition of the powder alloy and coatings before and after oxidation;

– experimental data on the microhardness of the powder alloy and coatings before and after oxidation;

– results and conclusions.

7. Approximate list of publications:

8. Date of issue of the assignment: 03.02.2020 р.

Calendar plan

item No	The name of the execution stages of Master's Thesis	The term of the practice stages	Note
1	2	3	4
1	Patent information search. Analysis of literature data and writing a review	03.02.20–06.03.2019	
2	. Select and validate the chemical composition of high-entropy coatings	03.02.20–07.02.2020	
3	Deposition of HE coatings by Cold Spray (CS)	10.02.2020	
4	Investigation of structure, phase and chemical composition of as CS coatings with SEM, EDX and XRD	10.02.2020-13.02.2020	
5	Vickers hardness measurements on PMT-3	13.02.2020	
6	Oxidation of the coatings in air at 900 °C for 100 h	11.02.2020-26.02.2020	
	Investigation of structure, phase and chemical composition of as oxidized CS coatings with SEM, EDX and XRD	28.02.2020-5.03.2020	
7	Vickers hardness measurements on PMT-3	28.02.20-5.03.2020	
8	Аналіз та узагальнення отриманих експериментальних результатів	11.03.20–30.04.20	
9	Розділ охорони праці	15.04.20–04.05.20	
10	Оформлення пояснювальної записки	11.03.20–04.05.20	
11	Оформлення графічної частини	30.04.20–04.05.20	

Undergraduate ______________ Olajide A.I.

Supervisor from the institution Yurkova A.I.

ABSTRACT

The master's thesis contains: 71 pages, 26 figures, 4 tables, 97 sources.

The purpose of the study is to investigate how high temperature oxidation treatment affects the structure, phase composition, microhardness, and corrosion properties of cold-sprayed AlNiCoFeCrTi high-entropy coatings. In order to achieve this purpose the following tasks are solved: The Microstructural Characterization, XRD patterns of cold spray coatings, SEM Micrographs of Cold Spray and Microhardness of the high entropy coatings.

The objective of research is to study the structure, phase composition, microhardness of cold sprayed AlNiCoFeCrTi coating when subjected to high temperature oxidation.

The aim of the research is to investigate how high temperature oxidation treatment affects the structure, phase composition, microhardness of cold-sprayed AlNiCoFeCrTi high-entropy coatings.

Research methods and equipment: The mechanical alloying was carried out in a planetary ball mill. Spraying was performed on a DYMET 405 setup. The structure and phase composition were studied using a scanning electron microscope, REMMA--106И, and an Ultima IV X-ray diffractometer f. Rigaku. Microhardness was determined by indentation on a PMT-3 device.

Scientific novelty of the results:

– it was found that AlNiCoFeCrTi cold sprayed HE coatings were successful in preventing the Fe based ($Fe_{18}Cr$) and Ni based ($Ni_{25}Cr$) substrates oxidation at 900 °C for 100 h
– The oxidated HEA coating exhibits high hardness HV=6,5 GPa.
– it was shown that, in contrast to under oxidation of the AlNiCoFeCrTi cold sprayed HE coatings Ni based substarte tends to oxidate faster than that on the Fe based substrate

CONTENT

INTRODUCTION

Cold spraying (CS) is a coating deposition method. Solid powders (1 to 60 mm in diameter) are accelerated in a supersonic gas jet to velocities up to ca. 1200 m/s. During impact with the substrate, particles undergo plastic deformation and adhere to the surface.

To achieve a uniform thickness the spraying nozzle is scanned along the substrate. metals, polymers, ceramics, composite materials and nanocrystalline powders can be deposited using cold spraying. The kinetic energy of the particles, supplied by the expansion of the gas, is converted to plastic deformation energy during bonding. Unlike thermal spraying techniques, e.g., plasma spraying, arc spraying, flame spraying, or high velocity oxygen fuel (HVOF), the powders are not melted during the spraying process.

In general, structural materials that are currently available for most of the application are based on a single principled element. Fe-based steels, Al-based alloys, Ni-based superalloys, etc. Although, solid solution strengthening by more than one solute in equi-molar proportions a viable option, processing of alloys based on multi-principal elements was not attempted for a long time on the notion that they may form complex compounds with complex structures.

The term “high-entropy” in HEAs originates from the resultant high entropy of mixed in equi-molar proportions. The HEAs formed with simple crystal structure have also shown strong properties such as high room temperature strength and strength retention at higher temperature.

There have been several processing routes to prepare HEAs, of which these includes casting, cold-spraying, sputtering, splat quenching, mechanical alloying (MA), and amidst those processes, HEAs prepared by casting route are widely studied. Based on metal structure and mechanical alloying (Ma) stable microstructures are as well. It is important to know aside certain contradiction of a single phase HEAs formed after mechanical alloying (MA), phase-separate (or precipitates other phases) during densification. In other to address these issues, in the present study, equi-atomic **AlNiCoFeCrTi**, were chosen for synthesis of HEAs by MA followed by densification. Alloying behavior of the above alloy during MA and after densification is studied by employing detailed characterization via X-ray diffraction (XRD) and scanning electron microscopy (SEM).

1 LITERATURE REVIEW

1.1 High entropy alloys as a novel concept of designing materials

High-entropy alloys (HEAs) are alloys formed by mixing five or more elements in equal or relatively large proportions (usually). Typical metal alloys had comprised one or two major components with smaller amounts of other elements prior to the synthesis of these substances.

For example, additional elements can be applied to iron to enhance its properties, producing an iron-based alloy, but usually in relatively low quantities, such as carbon, manganese, and the like in various steels [1]. Hence, high entropy alloys are a novel class of materials [1]–[2].

The term "high entropy alloys" was coined because the entropy increase in mixing is substantially higher when there is a greater number of elements in the mix, and their p roportions are approximately equal [3].

These alloys are currently the subject of significant attention in materials science a nd engineering because they possess potentially attractive properties.
However, research shows that some HEAs have considerably better strength-to- weight ratios, with a higher degree of fracture resistance, tensile strength, as well as corrosion and oxidation resistance than conventional alloys. Although HEAs have been studied since the 1980s, research substantially accelerated in the 2010s [1].

While HEAs were considered from a theoretical point of view as early as 1981 [4] and 1996 [5] and throughout the 1980s, Jien-Wei Yeh came up with his idea in 1995 about ways to actually create high-entropy alloys while driving through the countryside of Hsinchu, Taiwan. Shortly after he decided to start making certain special alloys of metal in his laboratory. With Taiwan being the only country that has been researching these alloys for over a decade, most other countries in Europe, the US and other parts of the world lagged behind in HEAs production.

Significant research interest from other countries did not develop until after 2004 when Jien-Wei Yeh and his team of Taiwanese scientists invented and built the first high-entropy alloys in the world capable of withstanding extremely high temperatures and pressures. Potential applications include use in state-of - the-art race cars, spacecraft, submarines, nuclear reactors, jet planes, nuclear weapons, long-range hypersonic missiles and so on [6].

A few months later, after Jien-Wei Yeh's paper was published, another independent paper on high entropy alloys was published by another British team composed of Brian Cantor, I. T. H. Chang, P. Knight and A. Vincent, J. B. Yeh was also the first to agree with the term 'high-entropy alloy' when he attributed high-configuration entropy as a mechanism for stabilizing the solid solution phase [7]. Cantor, unaware of Yeh's research, did not describe his alloy as a' high-entropy' alloy, but the base alloy he developed, FeCrMnNiCo equiatomic, was the subject of considerable work in the field [8].

Before classifying high entropy alloys and multi-component systems as a separate material class, nuclear scientists had already researched a system that can now be categorized as a high entropy alloy: Mo-Pd-Rh-Ru-Tc particles form at grain boundaries and at fission gas bubbles inside nuclear fuels [9]. Knowing the behavior of these '5 metal particles' was of particular interest to the medical industry as Tc-99 m is an important isotope for the medical imaging.

1.2 Core Effects in High Entropy Alloys

High entropy alloys have five or more major elements with four main effects: high entropy, sluggish diffusion, severe lattice distortion, and cocktail effects [1]. These effects give rise to certain distinct HEAs properties. Each effect will be discussed briefly.

1.2.1 High Entropy Effect

Although theoretically HEAs can form a large number of phases, due to the high-entropy effect, in fact only a few are produced. This influence plays an important role because it favors simple solid solution phases with FCC (face-centered cubic cell), BCC (body-centered cubic cell) and HCP (hexagonal closed-packed cell) [10].

High entropy effect is the most important effect since it can improve solid solutions creation and make the microstructure much simpler than expected [11]. The high-entropy effect states that the higher (mainly configurational) mixing entropy in HEAs lowers the free energy of solid solution phases and facilitates their formation, especially at higher temperatures. Because of this enhanced mutual solubility between constituent elements, the number of phases present in HEAs can be reduced apparently. According to $G = H - TS$ (where G is the free energy of Gibbs, H is enthalpy, T is temperature, and S is entropy) entropy may stabilize a higher entropy phase, provided the temperature is high enough. For example, a pure metal's melting phenomenon is due to the higher entropy of the liquid state relative to the solid state (according to Richard's rule, the entropy difference between the two states is roughly equal to the gas constant R at melting point) [1].

Likewise, those with higher entropy may also be stabilized at high temperatures between different types of phases in an alloy. Solid solution phases (including terminal and intermediate solid solutions) in conventional alloys have higher mixing entropy compared to intermetallic compounds [1]. For HEAs, due to the multi-principal element structure, the difference in entropy between solid solutions and compounds is particularly large. For example, the configurational entropy for a random solid equimolar quinary solution is 1.61R. This implies that the entropy difference between an equimolar quinary solution and a fully ordered phase (whose entropy is negligible) is about 60 percent greater than the above-mentioned entropy difference in the melting case (i.e. 60 percent greater than the entropy difference between liquid and solid pure metal states). So, solid solution phases are highly likely to become the stable phase in high temperature HEAs. The overall degree of order in HEAs is expected to decrease with increase in temperature. Thus, even those alloys in their cast state which contain ordered phases can turn at high temperature into random solid solutions. However, if an intermetallic compound's formation enthalpy is high enough to surpass the entropy effect, then that intermetallic compound will remain stable at high temperatures [12]. There is much evidence for the high entropy effect. This effect is shown in Figure 1.1, which shows the XRD patterns from a sequence of binary to septenary alloys. All the alloys have one or two major phases that have simple structures.

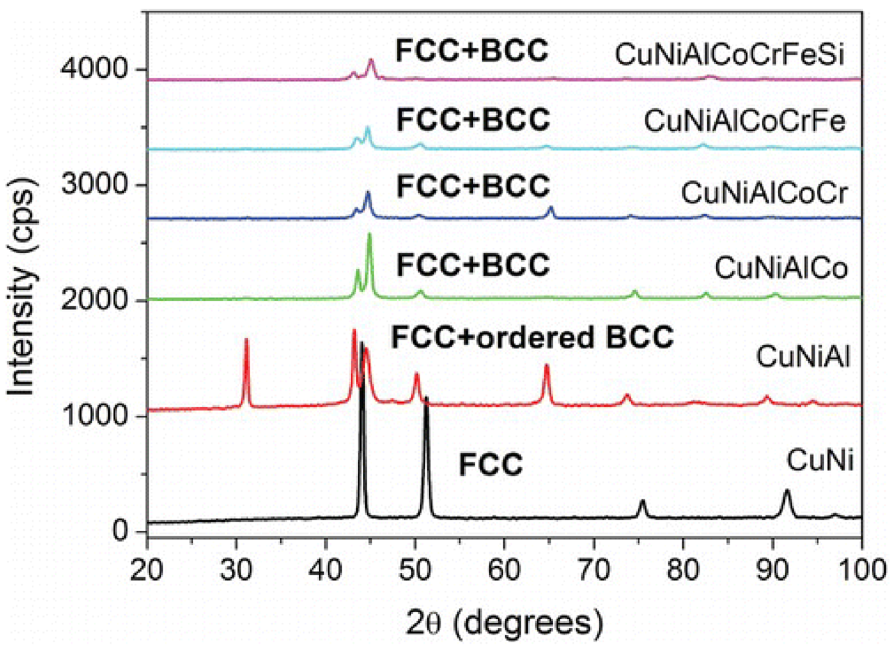

Figure 1.1 – The XRD patterns of a series alloy designed by the sequential addition of one extra element to the previous one [1]

It is seen that the phases in quinary, senary and septenary alloys remain very simple: there are only two major phases, and these phases have basic structures such as BCC and FCC (note that the seven alloy actually contains minor intermetallic phases, though not clearly seen in the XRD pattern). These basic structures contradict conventional expectations: the creation of binary / ternary compounds of various kinds [13]–[19].

Two myths about high entropy effect are discussed here. The first myth is that, at high temperatures, the high-entropy effect ensures the formation of a simple solid solution phase (order / disordered BCC / FCC). It's not real. Actually, the possibility of compound formation has already been stated in the very first HEA paper [7]. The presence of (Cr, Fe)-rich borides in the AlBxCoCrCuFeNi alloys was found in the same year [20]. As mentioned earlier, the phase formation is determined by the rivalry between entropy and enthalpy. The borides ' large negative enthalpy for formation thus supports their stability at high temperatures. Similar effects have also been found in other studies of annealing at high temperatures. The second myth is that the ideal phases for practical applications of HEAs are merely basic solid solution phases (BCC / FCC). This is not true, however. It's true that these simple solid solution phases, which are multi-principal-elements, are unique to HEAs and can have excellent properties. However, as shown later, there is also a great potential of HEAs which contain intermediate phases. Therefore, investigating HEAs should not be limited to simple phases of solid solutions [21]–[23].

1.2.2 Sluggish Diffusion Effect

The kinetics of diffusion and phase transition in HEAs have been suggested to be slower than those in their conventional counterparts [24]. This can be observed from two different aspects. Firstly, the neighboring atoms of each lattice site are slightly different in HEA. Therefore, before and after an atom leap into a vacancy the neighbors are different. The difference in local atomic configuration results in different bonding for each site, and hence different local energies. When an atom jumps into a low-energy site it becomes 'trapped' and there is less chance of jumping out of that site. In contrast, if the site is a high-energy site, then there is a higher chance that the atom will hop back to its original site. Both of these conditions slow the process of diffusion. Remember that the local atomic configuration before and after jumping into a vacancy is, most of the time, similar in conventional alloys with low solute concentration. Tsai et al. used a seven-bond model to calculate the effect on diffusion of the local energy fluctuation [25].

Tsai et al. showed that the mean potential energy difference between lattice sites for Ni atoms diffusing in Co–Cr–Fe–Mn–Ni alloys (which has a single-phase, FCC structure) is 60.3 meV, which is 50 percent higher than that in Fe – Cr – Ni alloys (Figure 1.2). The mean difference (MD) in potential energy after each migration for pure metals is zero, whereas that for HEA is the largest [25].

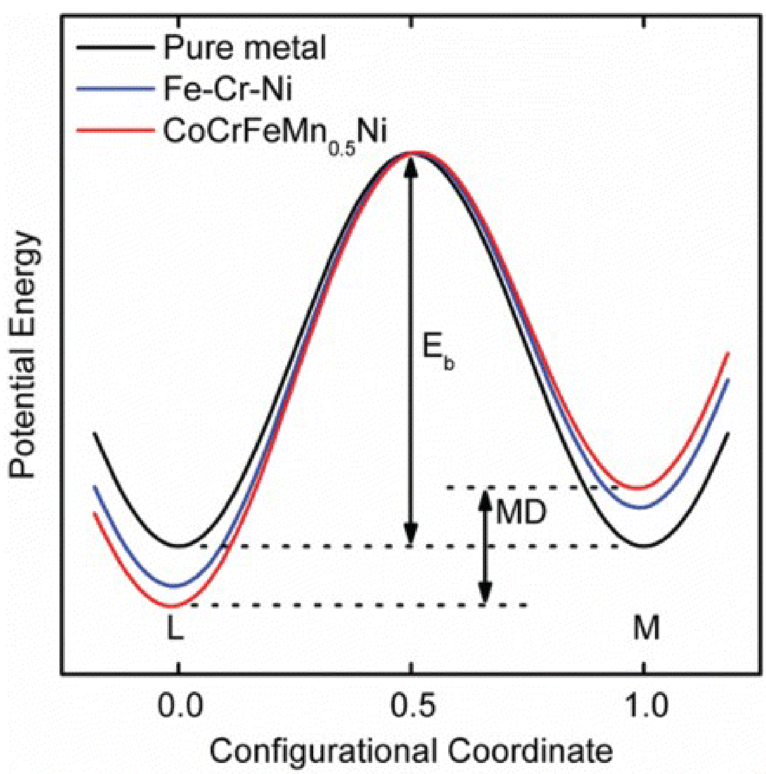

Figure 1.2 – Schematic diagram of the potential energy change during the migration of a Ni atom [25]

This energy difference results in a considerably longer period of occupation at low-energy sites (1.73 times longer than at high-energy sites). Indeed, diffusion couple experiments show that the activation energy of diffusion in the Co–Cr–Fe–Mn–Ni alloys is higher than in other FCC ternary alloys and pure elements (Table 1.1) [25]. Also calculated is the diffusivity of Ni at the respective melting point of each metal (Table 1). The slowest diffusion again occurs in alloys Co–Cr–Fe–Mn–Ni.

Table 1.1 – Diffusion parameters for Ni in different FCC matrices. The compositions of Fe-Cr-Ni(-Si) alloys are in wt.% [25]

Solute	System	D_0 ($10^{-4}m^2/s$)	Q (kJ/mol)	$T_m(T_s)$ (K)	Q/T_m	D_{Tm} ($10^{-13}m^2/s$)
Ni	CoCrFeMnNi	19.7	317.5	1607	0.1975	0.95
	FCC Fe	3	314	1812	0.1733	2.66
	Co	0.43	282.2	1768	0.1596	1.98
	Ni	1.77	285.3	1728	0.1651	4.21
	Fe-15Cr-20Ni	1.5	300	1731	0.1733	1.33
	Fe-15Cr-45Ni	1.8	293	1697	0.1727	1.73
	Fe-22Cr-45Ni	1.1	291	1688	0.1724	1.09
	Fe-15Cr-20Ni-Si	4.8	310	1705	0.1818	1.53

Secondly, diffusion rate is different for each element in a HEA. Many elements are less active (elements with high melting points for example) than others so these elements have lower success rates when competing with other elements to jump into vacancies. Nevertheless, phase transformations typically require several kinds of elements to be diffused coordinately. For example, to achieve the desired composition, nucleation and growth of a new phase involves the redistribution of all the elements. Grain growth often requires all elements to cooperate in order for the grain boundaries to migrate successfully. The slow-moving elements in those cases become the rate-limiting factor that impedes the transformation. The slow kinetics in HEAs permit easily attainable supersaturated state and nano-sized precipitates, even in cast state [7],[26]-[27]. It also contributes to the excellent performance of HEA coatings as diffusion barriers [28]. In addition, this allows for better high-temperature strength and structural stability. HEAs are also expected to exhibit excellent creep resistance for the same reason [29].

1.2.3 Severe-Lattice-Distortion Effect

In HEAs, the lattice consists of many types of elements, each with different sizes. These differences in size inevitably lead to lattice distortion. Larger atoms push their neighbors away and smaller ones have extra space around. The strain energy associated with distortion of the lattice elevates the HEA lattice's total free energy. It also has an effect on HEAs properties. For example, distortion of the lattice impedes motion of dislocation and leads to a pronounced strengthening of a solid solution. It also results in increased dispersion of propagating electrons and phonons, resulting in lower electrical and thermal conductivity [30].

Figure 1.3 shows a schematic representation of this effect with one element, two elements (where elements are very different in atomic sizes) and lattice structure with multi-elements. The stress-strain field, however, is not only affected by different sizes of compound elements but also by the energy of the bonds between them. Stronger bonds tend to have less bonding distances than weaker bonds. Because of this consequence, the lattice's strain energy increases and thus the lattice's total free energy increases as well. Furthermore, stress field is not uniform in the lattice and therefore HEAs have local stress gradients that slow down ion movement and are responsible for sluggish diffusion. Lattice distortion effect is very important, as it determines whether the phases of the solid solution are stable. If HEAs are composed of elements that cause too high the energy of the lattice distortion to retain the crystal structure, it collapses to an amorphous structure [1], [10]

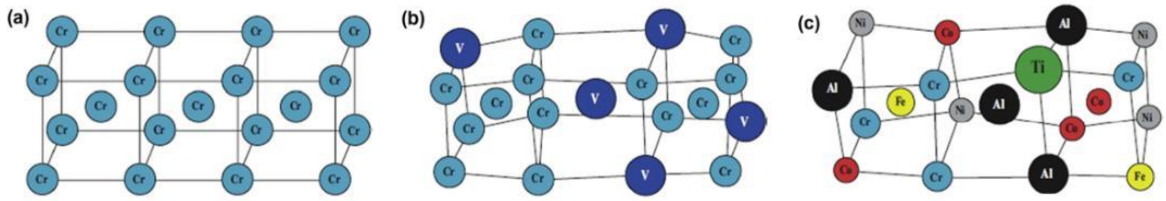

Figure 1.3 – Schematic representation of a BCC lattice with a) one element (Cr), b) two elements (Cr, V) and c) six elements (Cr, Ni, Fe, Co, Al, Ti), where atoms are distributed randomly [10]

This effect affects the materials mechanical, thermal, electric, optical and chemical behavior. It causes high strength for solid solutions (especially for BCC lattice HEAs), high thermal and electrical resistance, tensile brittleness and diffuse X-ray dispersion. Figure 1.4 illustrates schematically how the optical properties change as a result of distortion of the lattice. In Fig. 1.4(a) X-ray beams are reflected on a single-element alloy from Braggs planes, where the path of diffracted beams from both Bragg planes are same. In Fig. 1.4(b) diffracted beams from the Bragg planes multielement material diffract in various directions [1], [7], [31]

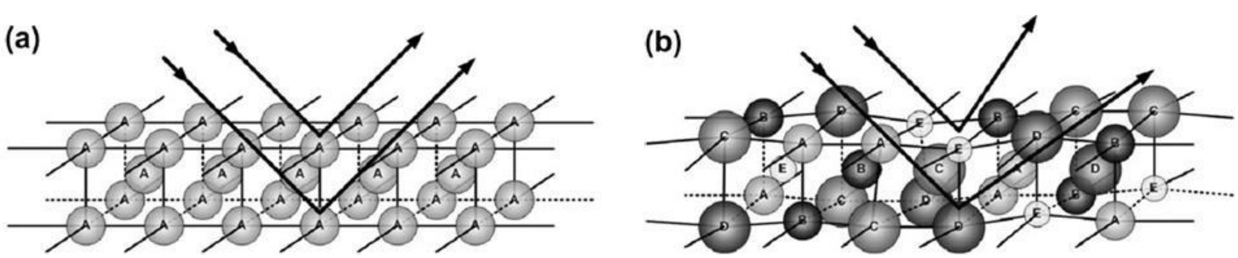

a) one-element lattice and b) multielement lattice

Figure 1.4 – X-ray diffraction on one-element lattice and multielement lattice [10]

The more elements that are in the alloy, the greater the distortion of the lattice and diffraction of X-rays. The X-ray diffraction intensities of alloys with more elements are therefore smaller than those with fewer elements under the same X-ray diffraction experimental conditions and geometry of the specimen [31].

1.2.4 Cocktail Effect

Certainly, the properties of HEAs are related to the properties of its composing elements. Adding light elements for example reduces the alloy density. Nevertheless, the relationship between the component elements should also be considered, in addition to the properties of the individual composing elements. For example, Al is a soft element with low melting point. However, adding Al can actually toughen HEAs [1].

Figure 1.5 plots the $Al_xCoCrCuFeNi$ alloy hardness as a function of the content of Al.

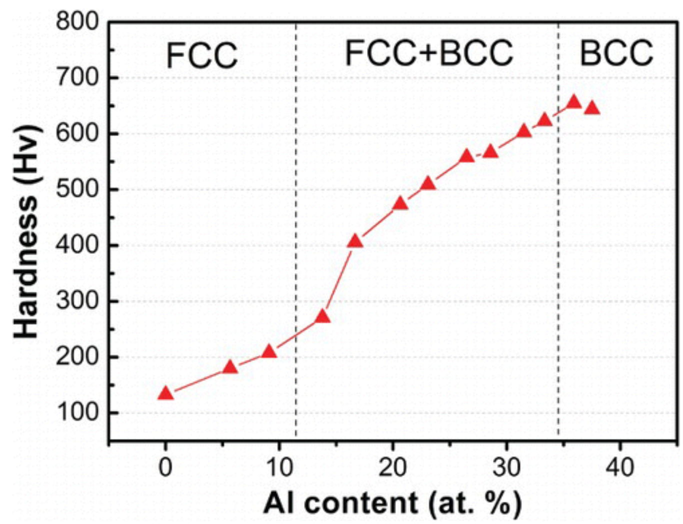

Figure 1.5 – Hardness of the $Al_xCoCrCuFeNi$ alloys as a function of Al content [1]

It's clearly seen that with the addition of Al, the alloy hardens significantly. This is due in part to the formation of a hard BCC phase, and in part to the stronger cohesive bonding between Al and other elements, as well as its greater atomic size. The macroscopic properties of HEA thus come not only from the average properties of the component elements, but also from the effects of the excess quantities created by inter-elemental reactions and distortion of the lattice [1].

1.3 Phases and Crystal Structure

Phases are typically classified in conventional alloys into three types: terminal solutions, intermediate solutions, and intermetal compounds. Different but extended concepts can be used to classify phases into HEAs. The terminal phases are phases that are based on a single dominant element. There is no change in the definition of intermetallic compounds: they are stoichiometric and have a fixed composition ratio. Nonetheless, because HEAs phases usually have a spectrum of composition rather than a fixed ratio of composition, intermetallic compounds are rarely seen in HEAs. Phases of solution are phases which do not belong to the two above categories. This category includes both simple (e.g. BCC and FCC) and complex structures (e.g. Laves phase) based solid solutions [1].

In the literature, phases in HEAs are normally classified differently. These are often categorized as: random solid solution (e.g. FCC, BCC), ordered solid solution (e.g. B2 and L12), and intermetallic phases (e.g., phases of Laves). This classification can contribute to some ambiguity, since intermetallic phases can also be categorized as ordered solid solutions by definition they have ranges of composition and are usually ordered. Having this in mind, this suggest classifying the phases according to their structure (simple / complex) and order (ordered / disordered). A phase is said to be straightforward if its form is similar to or derived from FCC, BCC or HCP. Namely, the structures of cI2-W, cF4-Cu, and hP2-Mg and their ordered forms (superlattices) such as cP2-CsCl (B2) and cP4-AuCu3 (L12) are simple [32]. If a phase is not simple (e.g. phases of laves), it is said to be complex. Simple disordered phase (SDP), simple ordered phase (SOP), and complex ordered phase (COP) are now to become the three forms from above [32].

1.3.1 Thermodynamics of High-Entropy Alloys

The multi-component alloys Yeh developed also consisted mainly or entirely of solid solution phases, contrary to the expectations of earlier work in multi-component systems, primarily in the metallic glass sector [7],[33]. Yeh attributed this finding to the high configuration, or mixing, entropy of a random solid solution that contains several elements. Because $\Delta G = \Delta H - \mathbf{T}\Delta S$ and the lowest Gibbs free formation energy (G) phase will be the equilibrium phase, increasing the likelihood of stable phase (entropy) will increase. For a random ideal solid solution, the mixing entropy can be determined by [7]:

$$\Delta S_{mix} = -R \sum_{i=1}^{N} c_i \ln c_i \tag{1.1}$$

where R is an ideal gas constant, N is the number of components and c_i is the atomic fraction of component i.

From this it can be seen that alloys in which the components are present in equal proportions will have the highest entropy and will increase entropy by adding additional elements. A 5-component, equiatomic alloy will have 1.61R mixing entropy [7], [34].

However, entropy alone isn't enough in every system to stabilize the solid solution process. Mixing enthalpy (ΔH_{mix}) must also be taken into consideration. That can be measured using the following [35]:

$$\Delta H_{mix} = \sum_{i=1, i \neq j}^{N} 4 \Delta H_{AB}^{mix} c_i c_j \tag{1.2}$$

where ΔH_{ABmix} is the binary enthalpy of mixing for A and B [35]. Zhang et al. found, empirically, that ΔH_{mix} should be between –10 and 5 kJ / mol in order to form a complete solid solution [34]. Moreover, Otto et al. found that if the alloy contains any pair of elements that tend to form ordered compounds in their binary system, the multi-component alloy containing them is also likely to form ordered compounds [36].

Both of the thermodynamic parameters can be combined into a single, unitless parameter Ω [37]:

$$\Omega = \frac{T_m \Delta S_{mix}}{|\Delta H_{mix}|} \tag{1.3}$$

where T_m is the average melting point of the elements in the alloy. Ω should be greater than or equal to 1.1 to promote solid solution development [37].

1.3.2 Entropy and Enthalpy of Solid Solutions and of Intermetallic Phases

One fundamental and important question about HEAs is: what kind of phase and crystal structure will be formed when we mix together so many different elements? Simple structures (SDPs and SOPs) are the most commonly seen in as-cast HEAs, to the surprise of most people (see Fig. 1.1). Such simple phases derive from the aforementioned high-entropy effect. In addition to basic phases, various types of COPs are also found in HEAs, such as σ, μ, Laves, etc. [1]. Since HEAs are special to simple-solution phases with more than five elements, researchers have worked intensively to understand the conditions for their creation.

From the classic Hume-Rothery rules, factors affecting binary solid solutions include difference in atomic size, concentration of electrons, and difference in electronegativity [38]. In addition to these factors, enthalpy and mixing entropy are the most important phase formation parameters for HEAs. Zhang et al. [34] and Guo et al. [39] studied the effect of these parameters on the formation of HEAs in phases and obtained similar conclusions: the formation of simple or complex phases depends primarily on the mixing enthalpy (ΔH_{mix}), mixing entropy (ΔS_{mix}) and differences in atomic size (δ). The following conditions must be met simultaneously in order to form single simple phases (i.e. FCC, BCC, and their mixtures, including both ordered/disordered cases): ($-22 \leq \Delta H_{mix} \leq 7$ kJ / mol, $\delta \leq 8.5$ and $11 \leq \Delta S_{mix} \leq 19.5$ J/(K mol) [39]. This is shown in Figure 1.6, where the boundary of simple phases is indicated. Those conditions are quite logical: ΔH_{mix} can't be too high in value, as large positive ΔH_{mix} results in phase separation, and large negative ΔH_{mix} typically leads to intermetallic phases. δ has to be small enough since large δ leads to excess strain energy and destabilizes simple structures. ΔS_{mix} has to be large enough because it is the main stabilizing factor for simple phases. If the target of discussion is limited to SDPs only, the conditions are more strict: $-15 \leq \Delta H_{mix} \leq 5$ kJ/mol, $\delta \leq 4.3$, and $12 \leq \Delta S_{mix} \leq 17.5$ J/(K mol) [34].

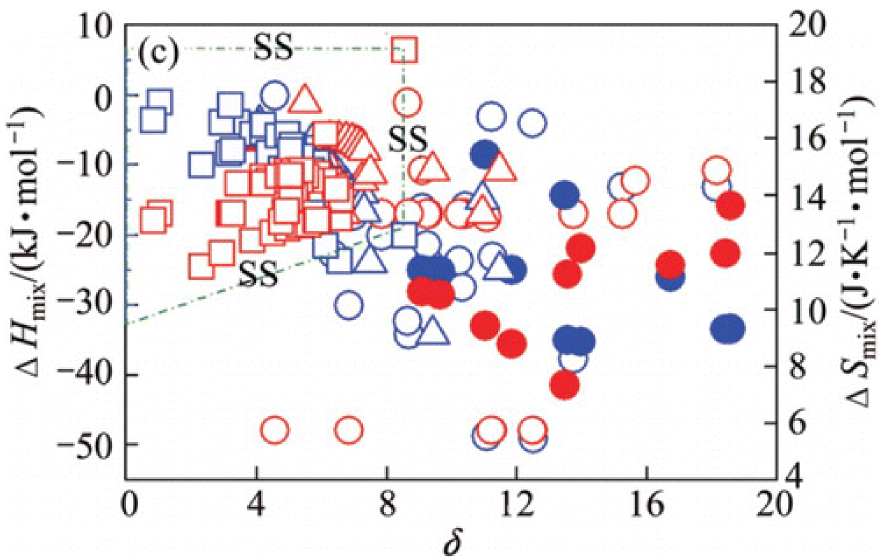

Figure 1.6 – Superimposed effect of H_{mix}, δ, and S_{mix} on phase stability in equiatomic multicomponent alloys and BMGs [39]

Notes to Fig. 1.6: Blue symbols indicate the relationship between H_{mix} and δ, while red ones represent that between S_{mix} and δ. Symbol ○ represents equiatomic amorphous phase-forming alloys; ● represents nonequiatomic amorphous phase-forming alloys; □ represents simple phases and Δ represents intermetallic phases. The region delineated by the dash-dotted lines indicates the requirements for simple phases to form [39].

The differences in atomic radii or size factor, δ, can be calculated using the following [39]:

$$\delta = 100\sqrt{\sum_{i=1}^{n} c_i \left(1 - r_i / \bar{r}\right)^2}, \tag{1.4}$$

here, $\bar{r}$ is the average of atomic radii (r_i) of all the components and is given by $\bar{r} = \sum_{i=1}^{n} c_i r_i$, and c_i is the atomic percentage of the i-th component.

1.3.3 Gibbs Phase Rule

Gibbs free energy G is a thermodynamic potential used to measure the work performed at a constant temperature and pressure by a thermodynamic system. The following applies for the Gibbs free energy: G = H − TS, where H is the enthalpy, and where S is entropy of the system. In stable phase, the difference between the elemental and the mixed state in the free energy of the Gibbs is minimal. Note: ΔG_{mix} as the Gibbs free energy of mixing, ΔH_{mix} as the mixing enthalpy, T as the absolute temperature and ΔS_{mix} as the mixing entropy. The temperature is clearly of great importance for the determination of stable phases in HEAs. Nevertheless, it should be emphasized that it is the competition between the mixing enthalpy and the mixing entropy that defines the formation of phases and is thus a strong parameter for predicting mutual solubility in solid solution phases [10],[40].

1.4 Phase Formation Rules and Phase Prediction for HEAs

The phase formation rules and phase prediction for HEAs would be viewed under the subsequent sub-topics:

1.4.1 Thermodynamics and Geometry Effect

If kinetic factors are not involved, the formation of phase is thermodynamically controlled by the Gibbs free energy, G, which is related to enthalpy, H, and entropy, S, in the case of mixing elemental components alloys:

$$\Delta G_{mix} = \Delta H_{mix} - T\Delta S_{mix},$$

here ΔG_{mix} the free energy of mixing Gibbs, ΔH_{mix} is the enthalpy of mixing, ΔS_{mix} the entropy of mixing, and T is the temperature at which various elements are mixed.

Note, that the term ΔS_{mix} include all entropy sources such as configurational, vibrational, electronic and magnetic contributions. Naturally, the phase selection in HEAs is decided by the competition between ΔH_{mix} and $T\Delta S_{mix}$. This is the thermodynamic consideration of the rules relating to phase formation. Another significant effect when considering the phase formation is the effect of geometry or, more specifically, the effect of atomic size. (See 1.3.1 and 1.3.2 for more information and on mixing of enthalpy and entropy and also it's differences in atomic radii). [7], [33]-[39].

1.4.2 Valence electron concentration

The most critical factor that determines whether an alloy crystallizes into a BCC or FCC structure tends to be its VEC (valence electron concentration, an alloy's VEC is determined from the component's weighted average VEC). Guo et al. summarized VEC's relationship to the structure of many HEAs (Figure 1.7) [41] They found that the FCC structure is stabilized when the alloy's VEC is larger than 8. When the alloy's VEC is less than 6.87, it stabilizes the BCC structure. The coexistence of the FCC and BCC phases is observed at VEC values between 6.87 and 8. [41] However, the mechanism behind VEC's impact on the creation of phases has not yet been fully understood.

The valence electron concentration, *VEC*, was determined from [41]:

$$VEC = \sum_{i=1}^{n} c_i \cdot (VEC)_i, \tag{1.5}$$

where, c_i is the atomic percentage of the i-th component, (VEC)i is the valence electron concentration of the i-th component.

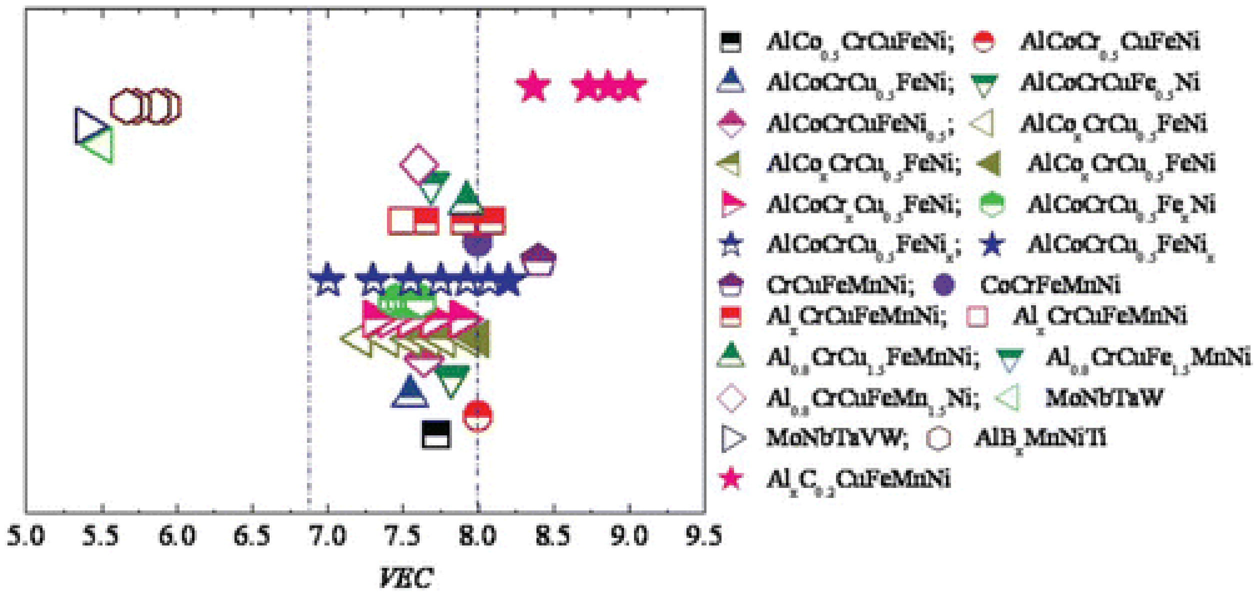

Figure 1.7 – Relationship between VEC and the FCC, BCC phase stability for various HEA systems [41]

Notes: Fully closed symbols for sole FCC phases; fully open symbols for sole BCC phase; top half-closed symbols for mixed FCC and BCC phases [41].

1.5 High-Entropy Alloys Properties

1.5.1 Mechanical Properties

It has been found that the crystal structure of HEAs is the primary factor in determining the mechanical properties. Bcc HEAs are typically high in yield strength and low in ductility, and vice versa for fcc HEAs. Certain alloys have been especially noted for their exceptional mechanical properties. VNbMoTaW, a refractory alloy, maintains a high yield strength (> 600 MPa (87 ksi)) even at a temperature of 1,400 °C (2,550 °F), which significantly outperforms conventional superalloys such as Inconel 718. Room temperature ductility, however, is low, less is known about other significant high temperature properties such as creep resistance and the alloy density is higher than conventional superalloys based on nickel [37].

CoCrFeMnNi was found to have outstanding mechanical properties at low temperatures and high fracture toughness, with both ductility and yield strength increasing as the test temperature dropped from room temperature to 77 K (−321.1 ° F). This was due to the advent of nanoscale twin boundary formation, an additional deformation mechanism not in action at higher temperatures. As such, it may have applications as a structural material in low-temperature applications or as an energy-absorbing material because of its high toughness [42]. However, later research has shown that lower-entropy alloys with fewer elements or non-equiatomic compositions may have higher strength [43] or higher toughness. [44] No ductile to brittle transition has been observed in the bcc AlCoCrFeNi alloy in tests as low as 77 K [37].

$Al_{0.5}CoCrCuFeNi$ was found to have a high limit on fatigue life and endurance, possibly exceeding some conventional alloys of steel and titanium. However, the results showed significant variability, suggesting that the material is very sensitive to manufacturing defects such as particles of aluminum oxide and microcracks [45].

A $Al_{20}Li_{20}Mg_{10}Sc_{20}Ti_{30}$ single-phase nanocrystalline alloy was developed with a density of 2.67gcm^{-3} and a microhardness of 4.9–5.8 GPa, which would give it an estimated strength-to-weight ratio comparable to ceramic materials such as silicon carbide [46] although the high cost of scandium limits possible uses [47]

Small-scale HEA samples (e.g. NbTaMoW micro-pillars) show extraordinarily high yield strengths of 4-10 GPa – an order of magnitude higher than that of its bulk form and their ductility is significantly improved. Additionally, these HEA films demonstrate significantly increased stability for long-lasting, high-temperature conditions (at 1,100 °C for 3 days). Combining these properties, small-scale HEAs represent a new class of materials in small-scale systems potentially suitable for high-stress and high-temperature applications [48]–[49].

New types of HEAs were produced in 2018 based on the careful placement of ordered oxygen complexes, a type of arranged interstitial complexes. Alloys of titanium, halfnium, and zirconium in particular have been shown to have enhanced characteristics of work hardening and ductility.

1.5.2 Wear and Fatigue Properties

Wear properties of HEAs were evaluated in a number of systems, under both abrasive and adhesive conditions [1]. Figure 1.8 illustrates adhesive wear properties of tested HEAs. HEAs consisting solely of SDPs typically show no better wear properties than conventional alloys with comparable hardness (e.g., compare $Al_{0.5}CoCrCuFeNi$ and 316SS in Figure 1.6). In the presence of certain B2 or COPs (e.g. $Al_2CoCrCuFeNi$ and $AlCoCrFe_{1.5}Mo_{0.5}Ni$) the wear resistance is clearly improved. When high-hardness COPs become the main phase, the resistance to wear is often excellent. Many HEA systems such as SKD61 tool steel (AISI H13) and SUJ2 bearing steel (AISI 52100) have comparable or even better performance than conventional wear-resistant alloys [51]-[52] For example, the $AlCoCrFeMo_{0.5}Ni$ alloy's wear resistance is comparable with SUJ2's (Figure 1.8). The $Al_{0.2}Co_{1.5}CrFeNi_{1.5}Ti$ alloy [51] in particular, has significantly greater wear resistance than SUJ2 and SKH51 (AISI M2, see Figure 1.8). The hardness is comparable to SUJ2's, but its resistance to wear is 3.6 times that of the latter. The $Al_{0.2}Co_{1.5}CrFeNi_{1.5}Ti$ alloy's wear resistance is half that of SKH51 but the latter's hardness is much higher. Outstanding performance at high temperatures is due to the higher HEA hardness. Additionally, since the wear mechanism is a mild oxidation wear, the stronger oxidation resistance in the alloy $Al_{0.2}Co_{1.5}CrFeNi_{1.5}Ti$ is also advantageous for its wear resistance [51].

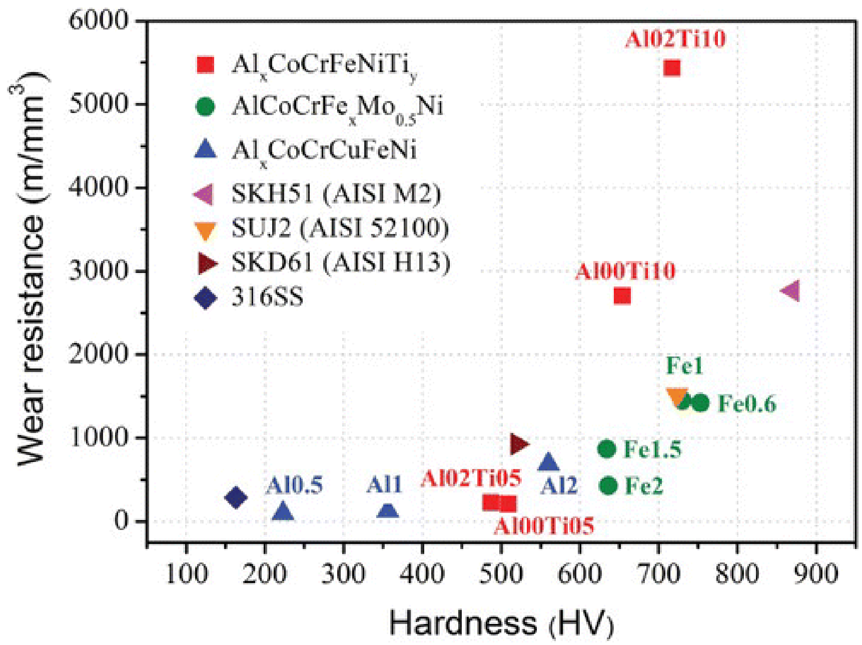

Figure 1.8 – Relationship between hardness and adhesive wear resistances of various HEAs and conventional alloys [51]–[52]

1.5.3 Corrosion Properties

Some HEAs have been tested for corrosion resistance in both NaCl and H_2SO_4 solutions [26], [53]. In both solutions, some HEAs show better corrosion properties than 304 SS and even 304L SS and have good pitting resistance [54]. Important factors include alloy composition and microstructure, in particular the quantity and distribution of corrosion resistant elements (such as Cr), and Most of the alloys tested are based on Co, Cr, Fe and Ni. The corrosion activity of the Co–Cr–Fe–Ni alloys is therefore first discussed, followed by the effect of elemental addition to the alloy system.

Corrosion in NACl Solution: CoCrFeNi single-phase FCC alloy in NaCl solution has significantly better corrosion resistance than 304L SS [55]. This is probably due to its high content of Cr and Ni. The addition of Cu to the CoCrFeNi alloy leads to the formation of a Cu-rich interdendrite phase that suffers from galvanic corrosion and severely degrades corrosion resistance [55]–[56]. To make matters worse, the passive film on the Cu-rich interdendrite regions does not provide good protection which further narrows down the passivation region [55]. The corrosion property can be improved by reducing the amount of Cu-rich phase by means of high-temperature annealing [56]. Adding 0.5 mole fraction of Al to the CoCrFeNi alloy results in the formation of (Al, Ni)-rich BCC phase and causes galvanic corrosion in the NaCl solution [53]. Al is also detrimental to the corrosion resistance of $Al_xCrFe_{1.5}MnNi_{0.5}$ alloys. The addition of Al significantly reduces the pitting potential and increases the region of localized / pitting corrosion in NaCl solution of these alloys [57].

Although it possesses higher pitting potential, the passive area is less than 304SS. The addition of Mo to the Co1.5CrFeNi1.5Ti0.5Mox alloy is advantageous because it naturally increases the pitting potential [58]–[59]. For example, the Co1.5CrFeNi1.5Ti0.5Mo0.1 alloy has a broad passivation region of 1.43 V in 1 M NaCl and has no pitting effect [59]–[60].

Corrosion in H_2SO_4 solution: CoCrFeNi also has a better corrosion resistance than 304 SS in H_2SO_4 solution [61]. The addition of Cu to the CoCrFeNi alloy reduces its corrosion properties. This is due to the formation of the Cu-rich phase, which is similar to the case in NaCl solution. It is also evident that the width of the passivation region is narrowed [54],[62]. The addition of Al is also harmful [57],[61] It leads to the formation of a two-phase FCC+BCC or BCC+B2 structure, in which the Ni, Al-rich BCC / B2 phase is preferentially corroded [61],[63]. In addition, the existence of Al makes the passive film porous and less protective [61]. Replacing Co with Mn in the Co–Cr–Fe–Ni alloy reduces its corrosion resistance in the H_2SO_4 solution and reduces its resistance to 304 SS [57]. The addition of B to the Al0.5CoCrCuFeNi alloy leads to the formation of Cr-rich borides and apparently reduces the Cr content of the matrix [62]. It makes the matrix far less resistant to corrosion. The addition of Ti to the alloy Co–Cr–Fe–Ni does not affect its outstanding corrosion behavior [59]. The addition of Mo to the alloy Co–Cr–Fe–Ni–Ti is detrimental to the corrosion resistance of the solution H_2SO_4. This is due to the formation of the (Cr, Mo)-rich σ phase, which decreases the concentration of

Cr in other phases [59]. AlCu0.5CoCrFeNiSi alloy has a better general corrosion resistance than 304 SS, but its area of passivation is smaller [54].

1.5.4 Oxidation Resistance

For conventional alloys, oxidation resistance could be significantly improved by adding appropriate amounts of Al, Cr, and Si, because at high temperatures, these elements could form dense and stable oxide layers on the surface (Sims and Hagel, 1972). By the same concept, many HEAs which contain these elements generally show better oxidation resistance. So AlCoCrFeNi and AlCoCrFeMoNi HEAs also show good resistance to oxidation up to 1100 °C. AlCrFeMnNi alloy is often less resistant to oxidation when the Mn content is higher [64].

The oxidation resistance of refractory HEAs is quite poor due to the strong affinity of refractory elements such as Ti, Zr, and Hf to oxygen but their oxides are not adherent by nature. Additionally, V oxide has low melting point, and Mo and W oxides have low boiling points. Senkov et al. (2012b) investigated the isothermal oxidation behavior of a refractory HEA CrMo0.5NbTa0.5TiZr during heating at 1273 K for 100 h in flowing air [64]. Continuous weight gain occurred during oxidation, and the time dependence of the weight gain per unit surface area can be described by a parabolic dependence with the time exponent n=0.6 [64]. The alloy has a better combination of mechanical properties and oxidation resistance than commercial Nb alloys and the developmental alloys NbSiAlTi and NbSiMo reported earlier.

Liu et al. (2014) studied four new HEAs, $Al_{0.5}CrMoNbTi$ (HTi), $Al_{0.5}CrMoNbV$ (HV), $Al_{0.5}CrMoNbTiV$ (HTiV), and $Al_{0.5}CrMoNbSi_{0.3}TiV$ ($HTiVSi_{0.3}$), respectively [64]. As anticipated, because of the high mixing entropy effect, these refractory HEAs consist mainly of a simple solid solution of BCC. But the oxidation kinetics of all the 1300 °C refractory HEAs follow a linear behavior despite some differences in oxidation rate among them. With Ti and Si addition the oxidation resistance of the HEAs is significantly improved, but reduced with V addition. Improving the oxidation resistance of refractory HEAs is therefore still a very important issue for applications at high temperatures relative to superalloys. In another analysis, Zhu et al. (2014), using AlCoCrFeNi HEA as a binder, prepared completely dense Ti(C, N) cermets. We have shown that the HEA binder has much better resistance to oxidation than the easy Ni / Co binder (Figure 1.9) [64].

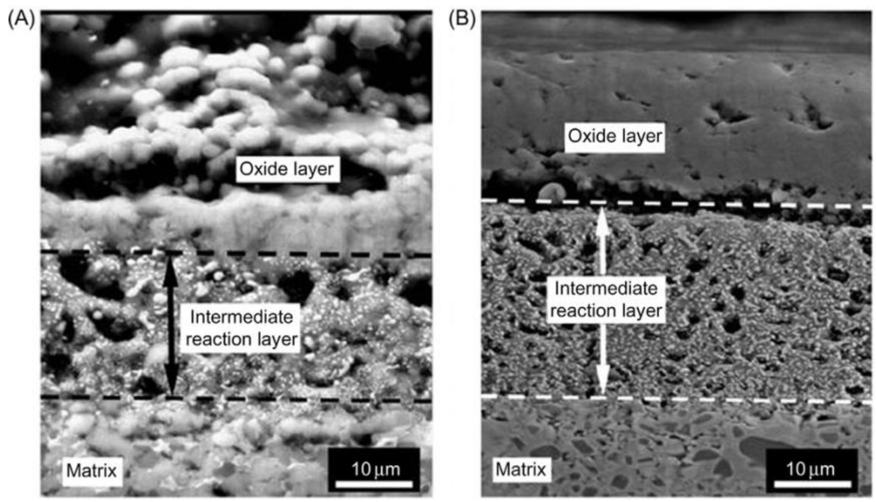

(A) Ni/Co and (B) AlCoCrFeNi HEA as binders

Figure 1.9 – Cross-sectional SEM images of Ti(C,N) cermet after isothermal oxidation at 1100 °C for 4 h in static air [64].

1.5.5 Irradiation Resistance

High-energy particle irradiation on solids is known to produce atomic displacements and thermal spikes. High atomic stresses in HEAs facilitate amorphization after irradiation of particles, followed by local melting and recrystallization due to thermal spikes; This process is speculated to leave far fewer defects in HEAs than in conventional alloys [65]. They may be excellent candidates for certain nuclear applications, for this reason. Egami et al. (2013) published initial results of computer simulation on model binary alloys and an electron microscopy analysis on

Hf-Nb-Zr alloys showing extremely high irradiation tolerance of these alloys to electron damage in support of this hypothesis [65]. Simulations on Hf-Nb-Zr alloys lead to the conclusion that HEAs with the volume strain near 0.1 at the atomic level are self-healing and highly resistant to irradiation [65].

1.5.6 Other Properties

The high multiple-element concentrations contribute to slow diffusion. For CoCrFeMnNi, the activation energy for diffusion was found to be higher for several elements than for pure metals and stainless steels, resulting in lower diffusion coefficients. [25] Several equiatomic multi-component alloys were also reported to show good resistance to energetic radiation damage [66]. High entropy alloys are investigated for applications for hydrogen storage [67]–[68].

1.6 Fabrication Routes

High-entropy alloy manufacturing processes may be categorized into three main routes [69]. The first route is from the liquid state, which involves arc melting, electric resistance melting, inductive melting, laser melting, laser cladding and Laser Enhanced Net Shape (LENS). The second route is from solid state, which mainly involves mechanical alloy (MA) and subsequent process of consolidation. We can combine the vapor state elements too. This route involves deposition of the sputter, deposition of the laser pulse (PLD), deposition of the atomic layer (ALD), epitaxy of the molecular beam (MBE), and deposition of the phase vapor to prepare the films on substrates [69]. Discussing below some routes from the three categories

1.6.1 Mechanical Alloying

Murty and the coworkers gave the first examples of solid solution HEAs prepared by MA. The Ph.D. thesis of S. Varalakshmi [70] reported the preparation of mechanical-alloy equiatomic elemental powder blends in AlFeTiCrZnCu, CuNiCoZnAlTi, FeNiMnAlCrCo, and NiFeCrCoMnW. The equiatomic binary to six-component compositions of all four systems was synthesized in the order of, for example AlFe, AlFeTi, AlFeTiCr, AlFeTiCrZn and AlFeTiCrZnCu. In non-equiatomic compositions, the effect of composition on HEA formation was also observed by varying one of the elements from 0 to 50 at.%. All alloys in these systems had either the phase BCC or FCC as the main phase as determined by X-ray diffraction. After annealing, the as-milled structures (BCC or FCC) were maintained for 1 h at 800 °C The nano-crystalline grain sizes (~10 nm) were shown in the as-milled structures, and the nano-structured grain size was maintained at 800°C after annealing [70]. Chen et al. subsequently researched the alloying behavior of binary to octonary alloys based on Cu-Ni-Al-Co-Cr-Fe-Ti-Mo prepared by mechanical alloy. Binary and ternary alloys respectively formed phases of FCC, or phases of BCC. Quaternary to octagonal alloys first developed solid FCC solutions which transformed after prolonged milling into amorphous structures [71].

Zhang et al. milled equiatomic AlCoCrCuFeNi. The as-milled powders were solid solutions with the structures of the BCC (major phase) and the FCC (minor phase). The grain size was very fine nanoscale with an estimated size of about 7 nm. BCC and FCC phases were given by annealing at 600 °C. Another FCC phase appeared after annealing at 1000 °C This was equivalent to the arc-melted and cast AlCoCrCuFeNi structures observed [72].

Praveen et al. prepared AlCoCrCuFe and CoCrCuFeNi equiatomic alloys by mechanical alloying followed by spark plasma sintering (SPS) at 900C to compact the powders. After mechanical alloying for 15 h, AlCoCrCuFe showed mostly BCC structure, with a minor FCC peak by X-ray diffraction. However, CoCrCuFeNi showed mostly the FCC phase with very small traces of BCC. The structures observed by X-ray diffraction after SPS were as follows: in AlCoCrCuFe on ordered BCC (B2) phase was dominant with small amounts of Cu-rich FCC phase and sigma phase, and in

CoCrCuFeNi, FCC phases were dominant with small amounts of sigma phase present. The authors suggest that the additional phases formed in these alloys are attributed to the influence of enthalpies of mixing, and configurational entropy is not sufficient to suppress their formation [69],[73]

1.6.2 Laser Cladding

Laser cladding uses a focused beam of laser energy as the heat source and by concentrating on a very small area, it can keep the heat-affected region of the substratum very shallow. This feature minimizes the chance of cracking, voids, and deformation, resulting in a fine microstructure and a metallurgical bond that is superior to thermal spray bond strength. To date, laser cladding coating materials are primarily focused on Co-or Ni-based superalloys, such as Inconel and Stellite alloys, but with relatively low hardness they are considerably expensive. The newly designed HEAs have shown great potential in applications where high strength, high hardness, high wear resistance or resistance to high temperature softening is needed. Some of these promising properties suit those of the commonly used Co-and Ni-based coatings with the low cost benefit [69]. The Laser cladding method schematic drawing is shown in Fig. 1.10a [74]

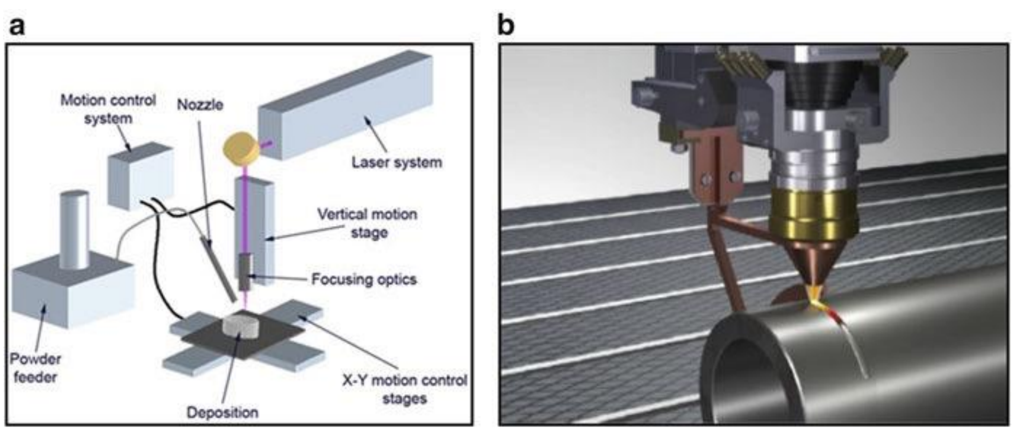

a – Schematic diagram; b – operation of laser cladding process

Figure 1.10 – Schematic diagram and operation of laser cladding process [74]–[75]

The basic system consists of a beam-generating laser source, a set of optics that direct and focus the beam, a powder feeder and a part manipulator. The laser and optics remain stationary, and the specimens move toward the laser. Fully automated laser cladding systems provide precise control of the cladding process. As the beam and powder injection are moved away, the melting pool formed by the laser beam quickly solidifies and becomes a completely dense weld bead [69]. Figure 1.10b is the method of laser cladding by filling materials in synchro-nous feeding mode [75]. Upon cladding, a single, overlapping multi-passed layer may be formed to protect the surface of the material. It can therefore be applied with a variety of sizes and shapes to all kinds of product and continues to gain market.

1.6.3 Physical Vapor Deposition

Physical vapor deposition (PVD) presents a variety of methods of vacuum deposition used to deposit thin films on different workpiece surfaces by condensing a vaporized form of desired film material. It includes deposition of the cathodic arc, deposition of physical vapor by electron beam, evaporative deposition, deposition by pulsed laser (PLD) and deposition by sputter [76]. The PLD operation is shown schematically in Fig. 1.11.

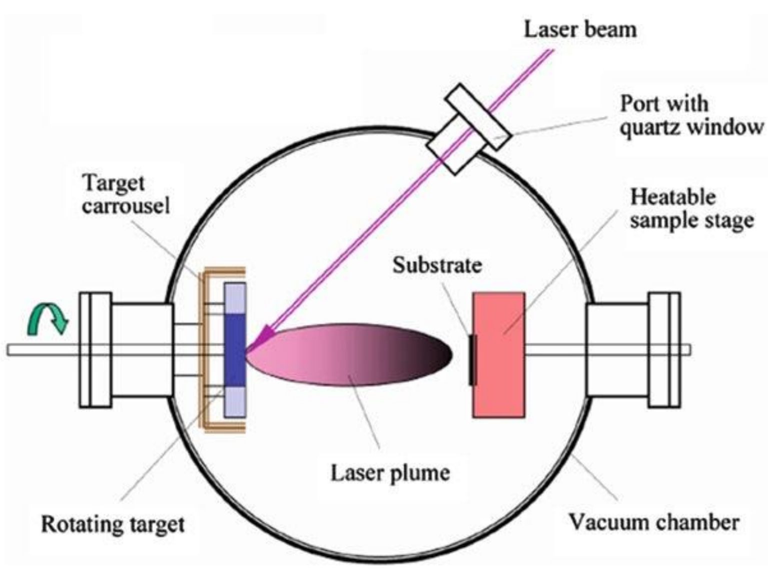

Figure 1.11 – A schematic showing the processing of pulse laser deposition [72]

PLD has been effectively used as another thin film deposition technique to deposit materials with multielements or complex stoichiometry [72] The required atomic fractions of the HEAs, a high-powered laser beam from the vacuum chamber hits the spinning target. Because of overheating, the vaporized energetic species from the target material, including atoms, ions, electrons and so on, are in the form of plasma plumes, which are further deposited on the substratum surface as a thin film [69],[72].

1.6.4 Thermal-Sprayed Methods

Thermal spraying techniques are processes of coating through which molten (or heated) materials are sprayed onto a surface. The "feedstock" (coating precursor) is heated using either electrical (plasma or arc) or chemical (combustion flame) means [78].

Thermal spraying can provide thick coatings (about 20 microns to several mm thickness ranges, depending on the method and feedstock) over a large area at a high deposition rate compared to other coating processes such as electroplating, physical and chemical vapor deposition. The thermal spray coating materials available include metals, alloys, ceramics, plastics, and composites. They are fed in powder or wire form, heated to a molten or semi-molten state, and accelerated in the form of micrometer-sized particles onto substrates. Combustion or discharge from the electric arc is typically used as the energy source for thermal spraying. Accumulation of multiple sprayed particles produces the resulting coatings. The surface may not heat up substantially, thereby allowing flammable substances to be coated. [78].

The quality of the coating is usually assessed by measuring its porosity, oxide content, macro and micro hardness, bond strength and roughness of the surface. The coating quality generally increases with increasing particle velocities [78].

1.6.4.1 Plasma Spraying

The material to be deposited (feedstock) – usually as a powder, sometimes as a liquid, suspension or wire – is inserted into the plasma stream, emanating from a plasma torch, during plasma spraying phase. In the jet, where the temperature is around 10,000 K, the material is melted and propelled into a substratum. There the molten droplets flatten, solidify quickly, forming a deposit. Commonly, the particles remain adherent to the substrate as coatings; it is also possible to produce free-standing sections by removing the substrate [78]. There are a large number of technological parameters that influence the particles ' interaction with the plasma jet and substratum, and thus the properties of the deposit. These parameters include type of feedstock, composition and flow rate of plasma gas, energy input, distance offset of the torch, cooling of the substrates, etc [78].

1.6.4.2 High Velocity Oxygen Fuel Spray (HVOF)

A class of thermal spray processes was developed during the 1980s, called high-velocity oxy-fuel spraying. A combination of gaseous or liquid fuel and oxygen is pumped into a combustion chamber, where it is continually ignited and combusted. The resulting hot gas emanates through a converging–diverging nozzle at a pressure close to 1 MPa and passes through a straight section. The fuels may be either gases (hydrogen, methane, propane, propylene, acetylene, natural gas, etc.) or liquids (kerosene, etc.) [78].

The jet velocity at the barrel exit (> 1000 m / s) is more than the sound velocity. A powder feed stock is pumped into the gas stream, speeding the powder to 800 m / s per second. The hot gas and powder stream is directed towards the coating surface. In the water the powder partly melts, and it settles on the soil. The resulting coating is of low porosity and high bond resistance [78]. Shown in Figure 1.12 is the schematic diagram of the high velocity oxygen fuel spray

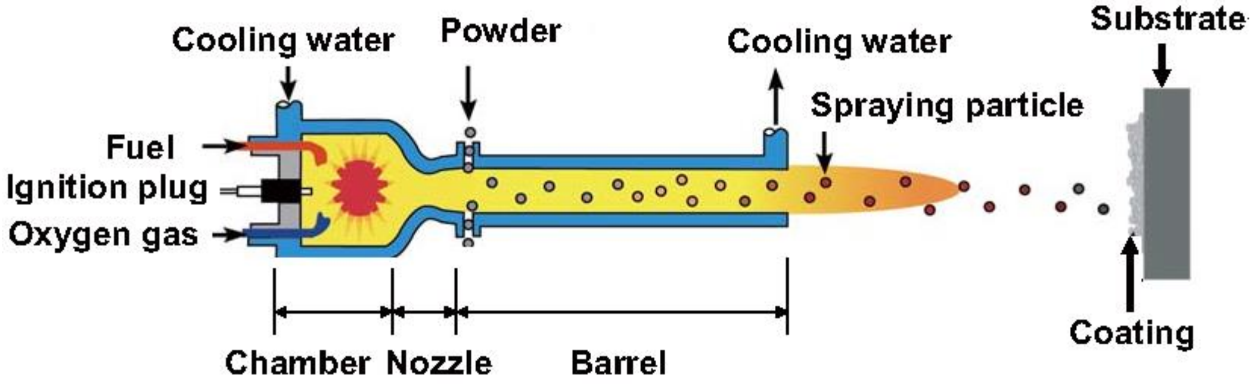

Figure 1.12 – HVOF Schematic [78]

Coatings with HVOF can be as thick as 12 mm (1/2) Typically, wear and corrosion resistant coatings are deposited on materials, such as ceramic and metallic layers. Common powders include WC-Co, MCrAlY, chromium carbide, and alumina. The most effective method was the deposition of cermet materials (WC–Co, etc.) and other corrosion-resistant alloys (stainless steels, nickel-based alloys, titanium, medical implant hydroxyapatite, etc.) [79]

1.6.4.3 Cold Spray process

In the 1990s, cold spray (or gas-dynamic cold spraying) was introduced to the market. The method was originally developed in the Soviet Union – while experimenting with target erosion, which was exposed to a high-velocity, two-phase fine powder flow in a wind tunnel, scientists observed accidental rapid coating formation [78]–[79].

In cold spraying, particles are accelerated to very high speeds by the carrier gas driven by a converging-diverging de Laval nozzle. Solid particles with sufficient kinetic energy deform plastically upon impact and mechanically bind to the substratum to form a coating. The critical velocity required to form bonding depends on the properties, powder size, and temperature of the material. Cold spraying may be used to deposit metals, polymers, ceramics, composite materials and nano-crystalline powders [80]. Soft metals such as Cu and Al are best suited for cold spraying, but other materials (W, Ta, Ti, MCrAlY, WC–Co, etc.) have been reported to be coated by cold spraying [79].

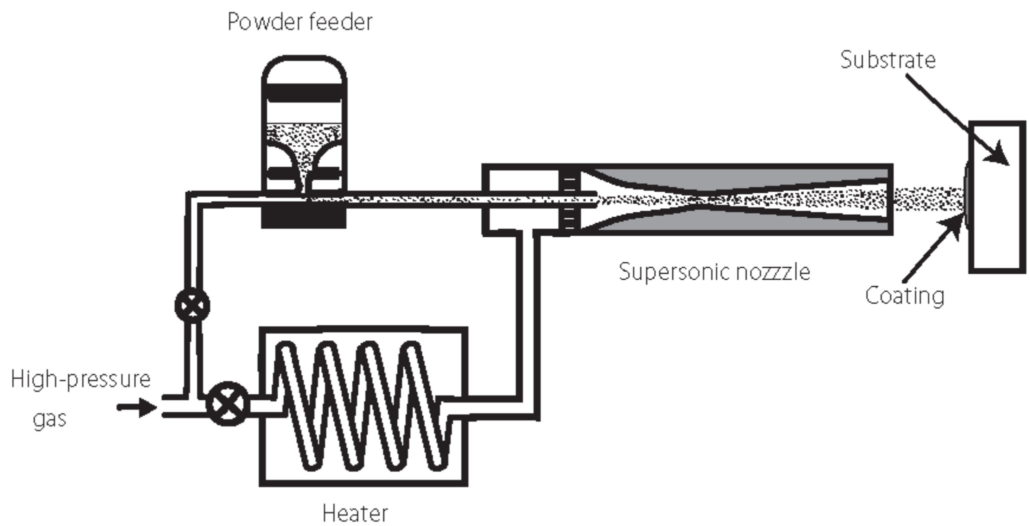

Figure 1.13– Cold Spraying Schematics [78]

The deposition efficiency for alloy powders is typically low, and the window of process parameters and appropriate powder sizes is narrow. Finer powders (< 20 micrometers) are used to accelerate the powders to higher velocity. Using a production gas with high sound rate (helium instead of nitrogen), it is possible to accelerate powder particles to much higher velocity. Helium, however, is volatile and is higher in flow rate, and thus in use. Nitrogen gas is heated up to around 900°C to boost acceleration strength. As a consequence, deposition quality and deposit tensile strength rise [78]–[79].

1.7 Potential Applications of High Entropy Alloys and High Entropy coatings

Several compositions have been developed and studied with the new concept of using high mixing entropy in alloy design. Many special types of HEAs have been reported including high entropy superalloys (HESAs), high entropy refractory alloys (HERAs), and high entropy metallic bulk glasses (HEBMGs). In addition, it has developed high entropy ceramics (HECs), such as high entropy carbides (HEACs), high entropy nitrides (HEANs), and high entropy oxides (HEAOs). Composites such as sintered carbide with HEA binders and cermets with HEA binders have also been reported recently [69]. It is very lucky that, as long as suitable choices are made, all the processes and methods used to prepare conventional materials can be applied to HE-related materials (HEMs). In addition, as long as the intended purposes are defined, various dimensions, facilities and apparatuses used to classify conventional materials can be used equally for HEMs. This is why scientists can easily access research and develop HEMs [69]. Furthermore, the combinations of compositions and processes are innumerable and could lead to a potentially wide range of microstructures and properties of HEMs and thus broad applications in various areas where conventional materials have been used [69].

1.8 Conclusions and statement of the research task

HEAs exhibit many unique and useful properties such as high hardness, excellent high temperature properties, mechanical properties, outstanding corrosion and wear resistance [7],[69] and are promising materials for industrial applications [7]. Surface modification in terms of coating deposition on the structural materials is a very effective method to enhance the wear and corrosion resistance which ultimately increase the service life of the materials. Practice of using HEA (nanocrystalline) coatings are being observed in recent days for long term surface protection of structural components in auto industry, nuclear industry, fireboxes of boilers, ships, etc. [7],[24]. Over 150 reports are available in the literature on HEA coatings, synthesized via the more popular laser cladding and sputtering (primarily for HEA nitride and carbide coatings) techniques, as well as by other thermal spray methods such as plasma spray and HVOF [24]. However, the advantage of cold spray in retaining the inherent alloy feedstock properties remains unmatched among all. Also, the information about the high temperature resistance to oxidation of HEA coatings obtained by cold gas-dynamic spraying is limited in nature.

Accordingly, the purpose of this study is to investigate how high temperature oxidation treatment affects the structure, phase composition, microhardness, and corrosion properties of cold-sprayed AlNiCoFeCrTi high-entropy coatings.

In order to achieve this purpose, the following tasks are decided in the work:

In order to achieve this purpose it is necessary to decide the following problems:

1) to select and substantiate the chemical composition of the powder mixture in order to obtain high-strength protective HEA coatings on a steel substrate;
2) to prepare powder mixture and steel substrates for coating by cold spraying;
3) to obtain a high-entropy AlNiCoFeCrTi coating on steel substrates by cold spraying;
4) to investigate the structure, phase, chemical composition and microhardness of cold-sprayed AlNiCoFeCrTi high-entropy coatings on steel substrates;
5) to conduct the isothermal oxidation at 900 °C for 100 hours on the AlNiCoFeCrTi coatings cold-sprayed on Ni- and Fe-base substrates;
6) to study the structure, phase and chemical composition of cold-sprayed AlNiCoFeCrTi coatings, as well as their microhardness after oxidation;
7) to analyze the results and draw conclusions.

2 EXPERIMENTAL MATERIALS AND PROCEDURES

2.1 The selection of alloy components for multicomponent HEA. Thermodynamic Parameters to Predict the Phase Formation

In order to select and substantiate the chemical composition of the powder mixture and to predict the phase composition of the AlNiCoFeCrTi HE alloy / coating , Using the Eq. 1.1-1.5 in the literature the entropy ΔS with the Boltzmann equation; mixing enthalpy ΔH; the difference of atomic radii δ; the valence electron concentration (VEC) were calculated.

Table 2.1 – The basic physical properties of the original elements [81]

Parameter	Elements					
	Al	Co	Ni	Fe	Cr	Ti
The atomic number	13	29	28	26	24	22
The atomic radius, nm	0,143	0,125	0,125	0,127	0,128	0,146
Melting point $T_{m.}$, °C	660	1495	1453	1538	1857	1660
Crystal structure	FCC	hexagonal close-packed (T<422°C) FCC (T>422°C)	FCC	BCC	BCC	hexagonal close-packed
VEC	3	9	10	8	6	4
Electronegativity χ_i	1,61	1,88	1,91	1,83	1,66	1,54

Table 2.2 – The enthalpy of mixing (bonding energy) for different atomic pairs (kJ / mol) [81]

Element	Al	Co	Ni	Fe	Cr	Ti
Al	–	−19	−22	−11	−10	−30
Co	−19	–	0	−1	−4	−28
Ni	−22	0	–	−2	−7	−35
Fe	−11	−1	−2	–	−1	−17
Cr	−10	−4	−7	−1	–	–7
Ti	−30	−28	−35	−17	–7	–

Table 2.3 – Solid solution criteria parameter values for multi-principle elemental AlNiCoFeCrTi HEA

HEA	Entropy of mixing, ΔS_{mix} (J/mol·K)	Enthalpy of mixing, ΔH_{mix} (kJ/mol)	Atomic size difference, δ (%)	Valence electron concentration, VEC (e/at)	Phase composition
AlNiCoFeCrTi	14.87	-21.38	7.25	6.64	BCC, intermetallic compounds

As summarized in Table 2.1, it can be concluded that the **AlNiCoFeCrTi** HEA contains **two** phases: besides bcc solid solution could contain intermetallic compounds because of large negative enthalpy.

From the different approaches [81], it can be said that there are still no universal criteria to predict the formation of different phase types. Even so, these approaches and predictions are very helpful for composition design with an aim to achieve required phase types such as solid solution (SS), partially ordered solid solution, intermetallic and so on.

2.2. Feed-stock powder for cold spraying

AlNiCoFeCrTi powder was prepared by mechanical alloying and annealing. Elemental Al, Ni ,Co, Fe, Cr, and Ti powders were mechanically alloyed in planetary-ball mill for 3h. Hardened steel-balls were used as the milling medium with a 10:1 ball-to-powder ratio in a hardened steel vial, and purified gasoline was used as the process control agent to avoid oxidation, cold welding, and excessive agglomeration.

The subsequent thermal annealing at temperature 1200°C during 1 hour was carried out. The powder agglomerates formed after annealing of AlFeNiCoCrTi HEA were subjected to grinding in a ball mill for 1 hour.

2.3. Cold Spray process for coating deposition

Cold spray (CS) is a method of deposition of solid-state material, which was originally developed in the 1980s as a coating technology [82]-[83]. High-temperature compressed gases (typically oxygen, air, or helium) are used in this phase as propulsive gas to accelerate powder feedstock (typically metals and metal matrix composites) to a high velocity (typically higher than 300 m / s) and to cause deposition when powders reach a substrate (typically metals). In contrast to conventional high-temperature deposition processes, the creation of a cold spray deposit relies primarily on the pre-impact particle kinetic energy rather than the thermal energy. During the whole deposition process the feedstock used for cold spray remains solid state. Deposition is accomplished by local metallurgical bonding and mechanical interlocking at the inter-particle and particle-substrate interfaces, caused by localized plastic deformation. This allows the avoidance of defects typically found in processes of high-temperature deposition, such as oxidation, residual thermal stress, and phase transformation [84–86]. Successful deposition of a cold sprayed deposit requires particles from the feedstock to reach a critical velocity of impact [87-91]. The creation of a deposit in cold spray consists of two distinct stages. The first stage includes the deposition of an initial layer of particles where there is bonding between feedstock particles and the substratum material; the second stage is the deposition on top of the previously deposited layer(s) where bonding occurs between feedstock particles. Each stage has its respective critical velocity, i.e. for bonding particles / substrate and for growth in deposits. Velocity of particle impact shall meet all conditions for successful deposition. In general, higher velocity of particles would result in improved quality of deposits. Remember that for both stages the critical velocity can be considered the same if the powder and substratum are the same material [87].

Deposition of powder AlFeNiCoCrTi high-entropy alloy was performed by CS process on a steel substrate using an air with a gun temperature and pressure of 400 °C and 0.7 MPa, respectively. The stand-off distance between the nozzle and the steel substrate was 30 mm. A commercial cold spray system (DYMET 405) was used in spraying experiments with compressed air. Shown in Fig 2.1 (a) and (b) are the images of the cold spray system and the compressor respectively.

(a) (b)

Figure 2.1 – (a) Cold Spray System (DYMET 405) and (b) Compressor

Processing conditions:

- Velocity of particle/gas jet – 700….1000 m/s,
- Process (propellant/carrier) gas – air, argon, N_2
- Gas pressure - 0,6 – 1.0 MPa,
- Standoff distance - about 10 mm,
- Inlet temperature – 200 - 600°C,
- Substrate - Quartz glass and/or steel

Impact of Particles and Substrate Here the illustration of the impart of the particles on the substrate is shown in Fig 2.2 below.

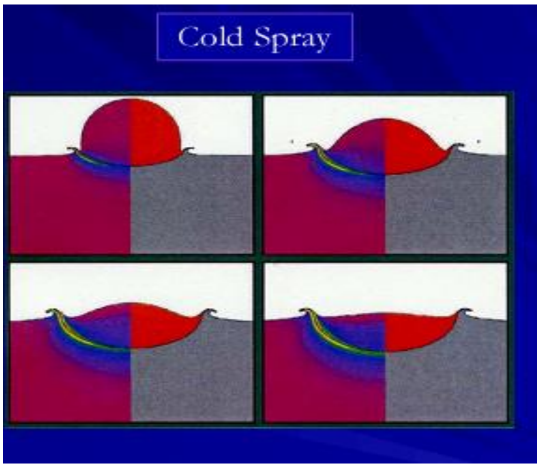

Figure 2.2 Particle impact site

When the particles impinge on the substrate three various phenomena can occur at different velocities, *V*:

- Low velocity v – particles scarred off
- Average velocity v – particle erosion
- High velocity v – particles deposit

The particles at limiting velocity varying with materials properties can be shown in Fig 2.3.

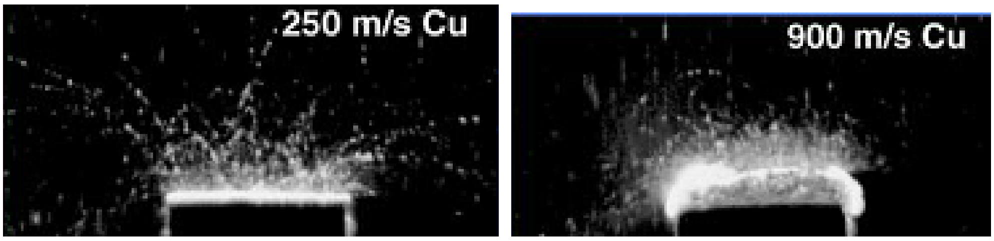

Figure 2.3 – The limiting velocity ‘v’ varies with material properties

Gas/particle v of 750 m/s (gas temperature 400 °C, gas pressure 0.7 MPa) was believed to be quite enough for deposition of AlNiCoFeCrTi HE coatings. Fig 2.4 shows the influence of the flow rate of the air-powder mixture on the mode of its interaction with the substrate

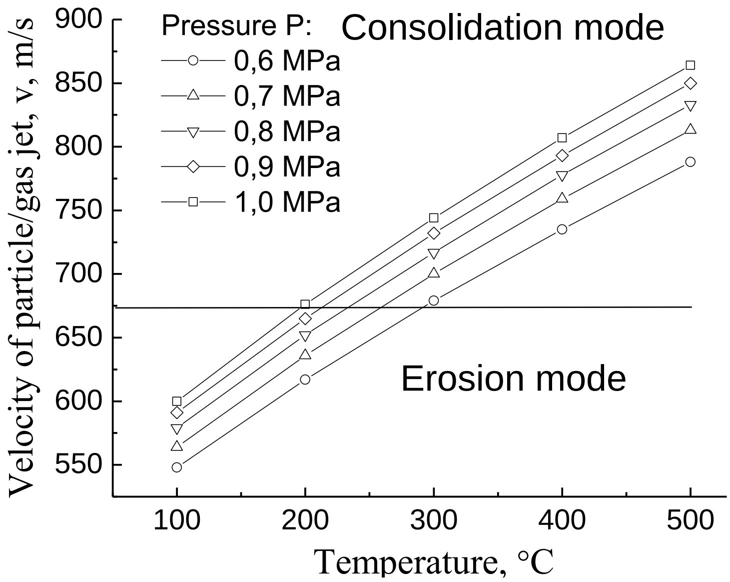

Figure 2.4 – The influence of the flow rate of the air-powder mixture on the mode of its interaction with the substrate

A cold rolled plate of steel (Fe18Cr and Ni25Cr) with a thickness about 3.0 mm was used as a substrate. Immediately prior to depositing the coatings, the substrate surface was prepared by SiC-blasting, rinsing, and then wiping with solvent to eliminate surface wetness.

2.4 Isothermal oxidation

Cold-sprayed AlNiCoFeCrTi coatings was oxidized in a laboratory scale muffle furnace in air at 900 °C for 100 h in a continuous isothermal fashion. After 100 h of oxidation, the samples were taken out from the furnace.

2.5 Characterization of Structure and Phase Composition

X-ray diffraction (XRD) analysis of the structure and phase composition of feed-stock powder and Cold Sprayed (CS) coatings before and after its oxidation was carried out with an Ultima IV X-ray diffractometer (Rigaku Co., Japan) in monochromatic Cu-Kα radiation and the working voltage and current were 30 kV and 20 mA, respectively. The monochromator was a graphite single crystal on the path of a diffracted beam. The diffraction patterns were taken by stepwise scanning at

2θ = (20 –120) °. The scanning angle was 0.04° and goniometer angular velocity was 2°/min. The X-ray diffraction data were processed with the Powder Cell 2.4 software for full-profile analysis of X-ray spectra. The lattice parameters of solid solutions were calculated according to the positions of the gravitation centers of the diffraction profiles by linear extrapolation method. The crystallite size (coherent-scattering region) in the milled powders as well as after consolidation by CS process has been calculated from the XRD peak broadening using peak profile analysis after eliminating the instrumental and strain contributions.

2.6 Microstructural Characterization

The microstructure of feedstock powder and CS coatings before and after its oxidation were examined with a scanning electron microscope (SEM). The chemical composition was determined with energy dispersive X-ray microanalysis (EDX) using SEM.

2.7 The particle size distribution

The particle size distribution was determined by Microtrac-Turbo Sync. The Sync interrogated wet particles with laser light; while, simultaneously, a high-speed digital camera took images. Samples were introduced to the FlowSync and dispersed throughout the system. Scattered light was captured with laser sequence across 165 degrees. Simultaneously, live images of the sample were taken with a highspeed digital camera.

2.8 Vickers Microhardness measurements

Vickers microhardness measurements were made on the coating cross-section before and after its oxidation using a Vickers microhardness machine PMT-3 under F= 1.5 N loading in compliance with standard procedure.

3. RESULTS AND DISCUSSION

3.1 Structural characterization of feed-stock powder of AlNiCoFeCrTi HEA for cold spraying

(XRD phase analysis; SEM micrographs of the powder)

Structural characterization of the feed-stock AlNiCoFeCrTi HEA powder used in cold-spraying process is shown in Fig. 3.1. below which illustrates the XRD patterns of the feed-stock powder after mechanical alloying for 1 hour after annealing at 1200 °C for 1 hour as shown below the diffraction peaks corresponding to a major disordered BCC solid solution β and TiC ♦ are visible and an intermetallic compound FeCr σ-phase peaks can be challenging to determine as it partially disappears in the AlNiCoFeCrTi alloy which strengthens bcc phase [93]. This dissolution is caused by increased difusion, even at low milling temperature, under the impact of severe plastic deformation.

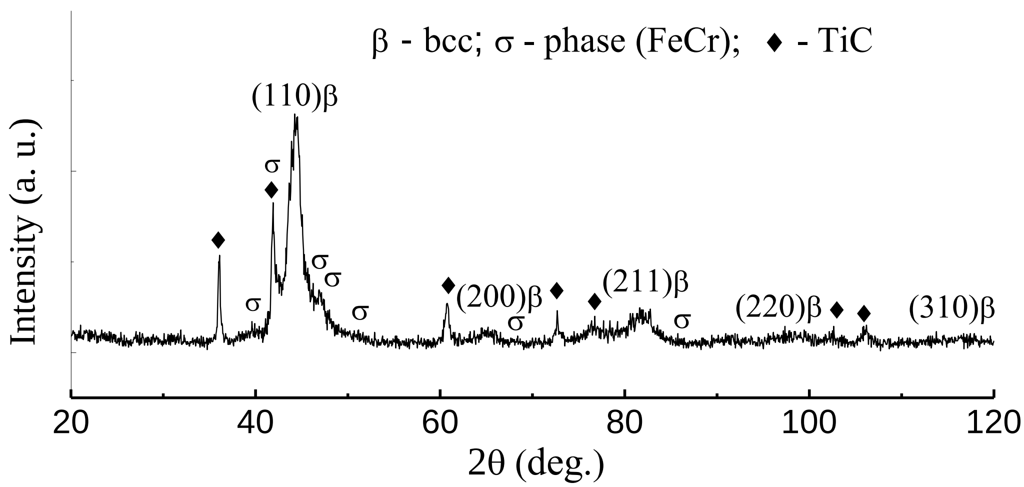

Fig. 3.1 – XRD patterns of the feed-stock AlNiCoFeCrTi HEA powder used in cold-spraying process

The morphology, microstructure and particle size distribution of AlNiCoFeCrTi HEA feedstock powders used for cold spray coating is shown in Fig. 3.2 a-c. The particles of powder are irregular in shape with a size range of 1–125 μm as shown in the size distribution map. From the Fig. 3b it can be seen that they are 3 phases: (i) the grey phase (major bcc solid solution), (ii) the light phase (σ-phase intermetallic compound FeCr) and (iii) the dark phase (TiC) [93].

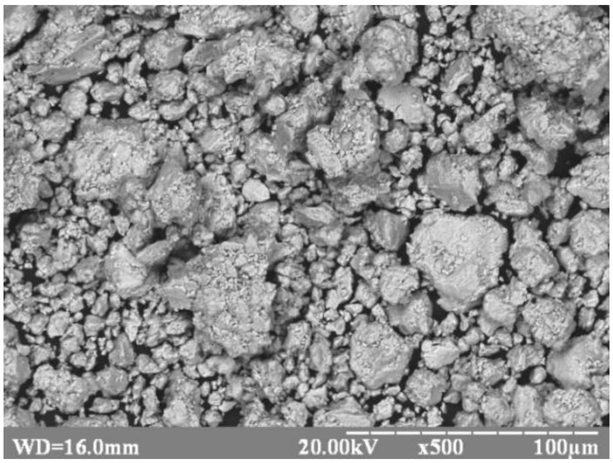

a

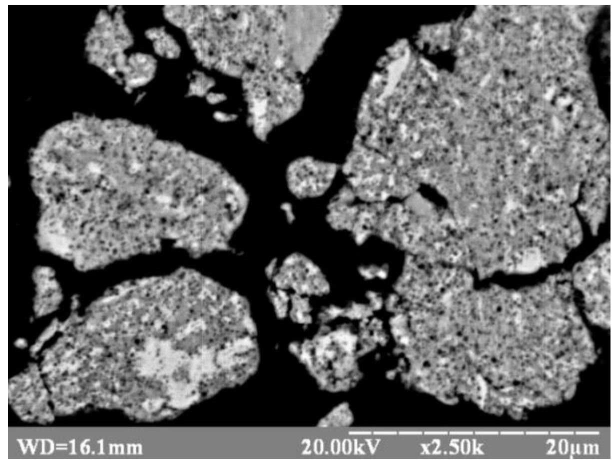

b

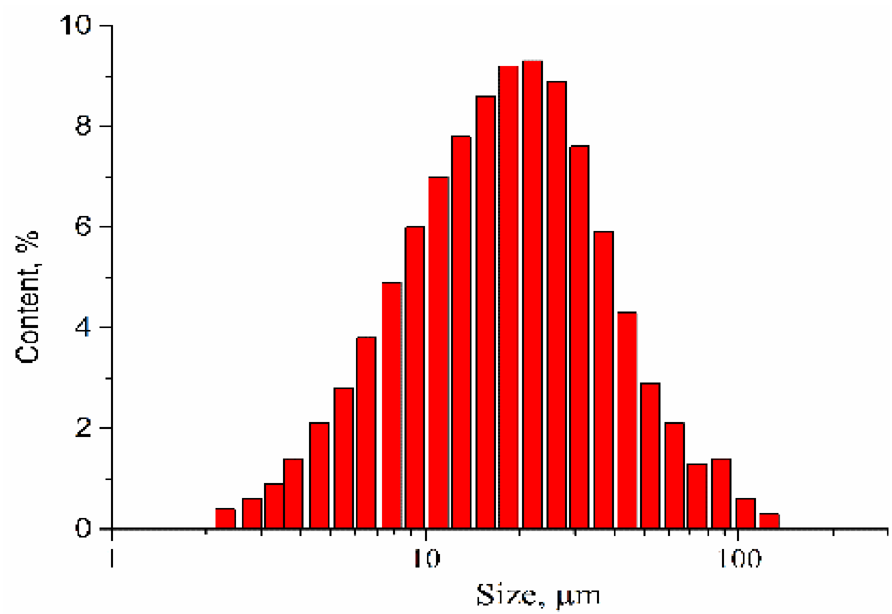

c

a – morphology; b – microstructure; c – particle size distribution

Figure 3.2 – SEM morphology and microstructure, and particle size distribution of the feed-stock AlNiCoFeCrTi HEA powder used in cold-spraying process

3.2. Structure Characterization of AlNiCoFeCrTi High-Entropy Cold Spraying Coatings

(XRD phase analysis, Cross-sectional SEM micrographs of the coating)

Coatings with average thickness about 400 μm and 130 μm were obtained on $Fe_{18}Cr$ and $Ni_{25}Cr$ substrates, respectively. Fig 3.3 shows a typical as-received AlNiCoFeCrTi CS coating.

Figure 3.3 – As-received AlNiCoFeCrTi CS coating

Figure 3.4 illustrates the XRD patterns taken on the top surface of the coating on $Fe_{18}Cr$ substrate before (Fig. 3.4a) and after (Fig. 3.4b) its oxidation at 900 °C for 100 h. The diffraction peaks observed from Fig. 3.4a shows they are 3 phases in the coating: (i) the disordered BCC solid solution β, (ii) intermellatic FeCr compound σ and (iii) TiC ♦ Comparing Fig 3.1 and Fig 3.4a shows little or no difference in their XRD pattern and consist of the same phases, the cold spray coating and the feed-stock diffraction peaks remains the same. The Fig 3.4b shows the XRD patterns of after oxidation where it can be seen the introduction of new phases compared to Fig 3.4a shows a major diffraction peaks of FCC and TiC and minor peaks of Al_2O_3 and disordered BCC. It is suggested that the dissolving of the disordered BCC gave rise to the Aluminium oxide, when the coating is been subjected to oxidation at high temperature Al, Cr and Fe tend to oxidize preferentially [94].

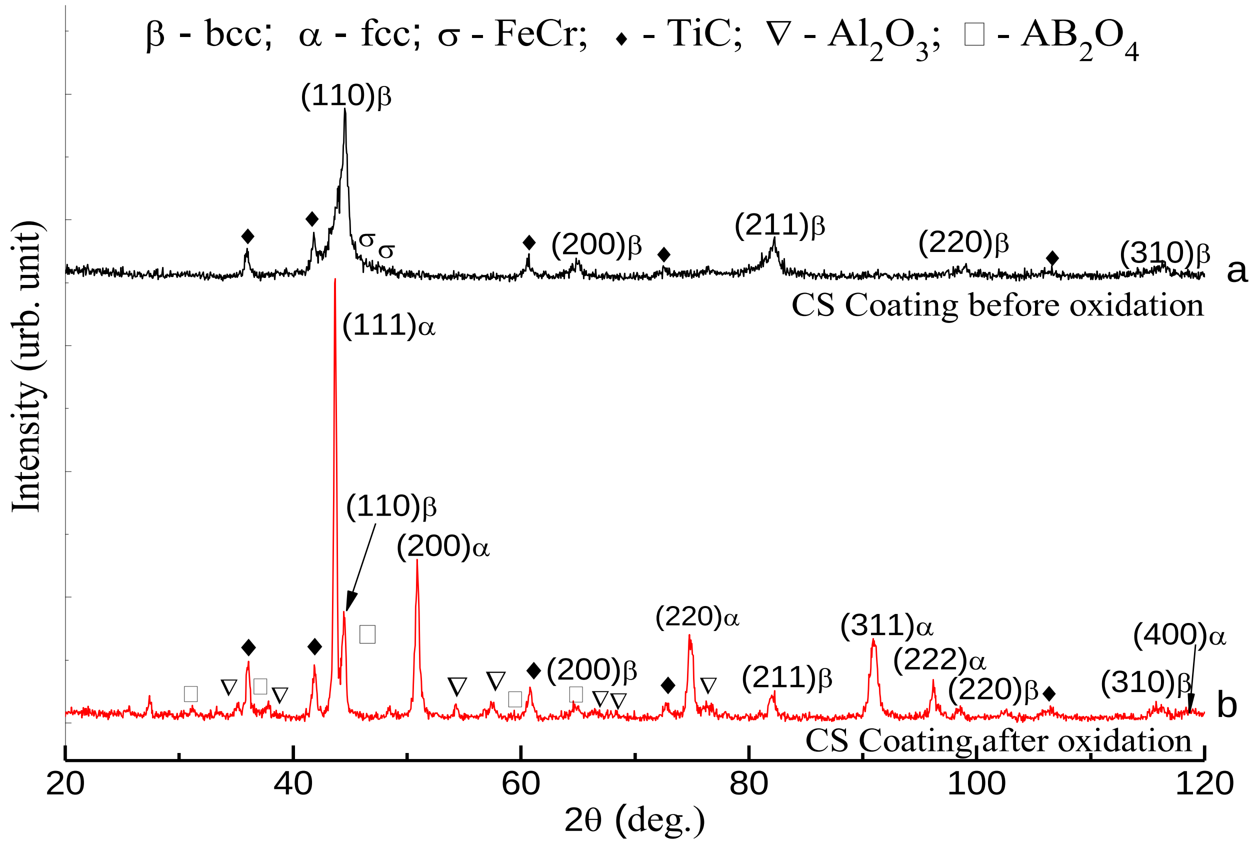

a – before oxidation, b – after oxidation

Figure 3.4 – XRD patterns of CS AlNiCoFeCrTi coating on $Fe_{18}Cr$ substrate before and after oxidation at 900°C for 100 h

Structural characterization of cold spray AlNiCoFeCrTi coating on $Ni_{25}Cr$ substrate before and after oxidation at 900°C for 100 h is shown in Fig. 3.5. The XRD patterns taken on the surface of the coating on $Ni_{25}Cr$ before oxidation shows little or no diffraction peaks of the σ-phase therefore showing main corresponding peaks of a disordered BCC solid solution and TiC as shown in Fig. 3.5a and the XRD pattern after oxidation Fig. 3.5b shows a more high intensity than the coating on the Iron based substrate giving rise to the same phases as that stated for Fig 3.4b

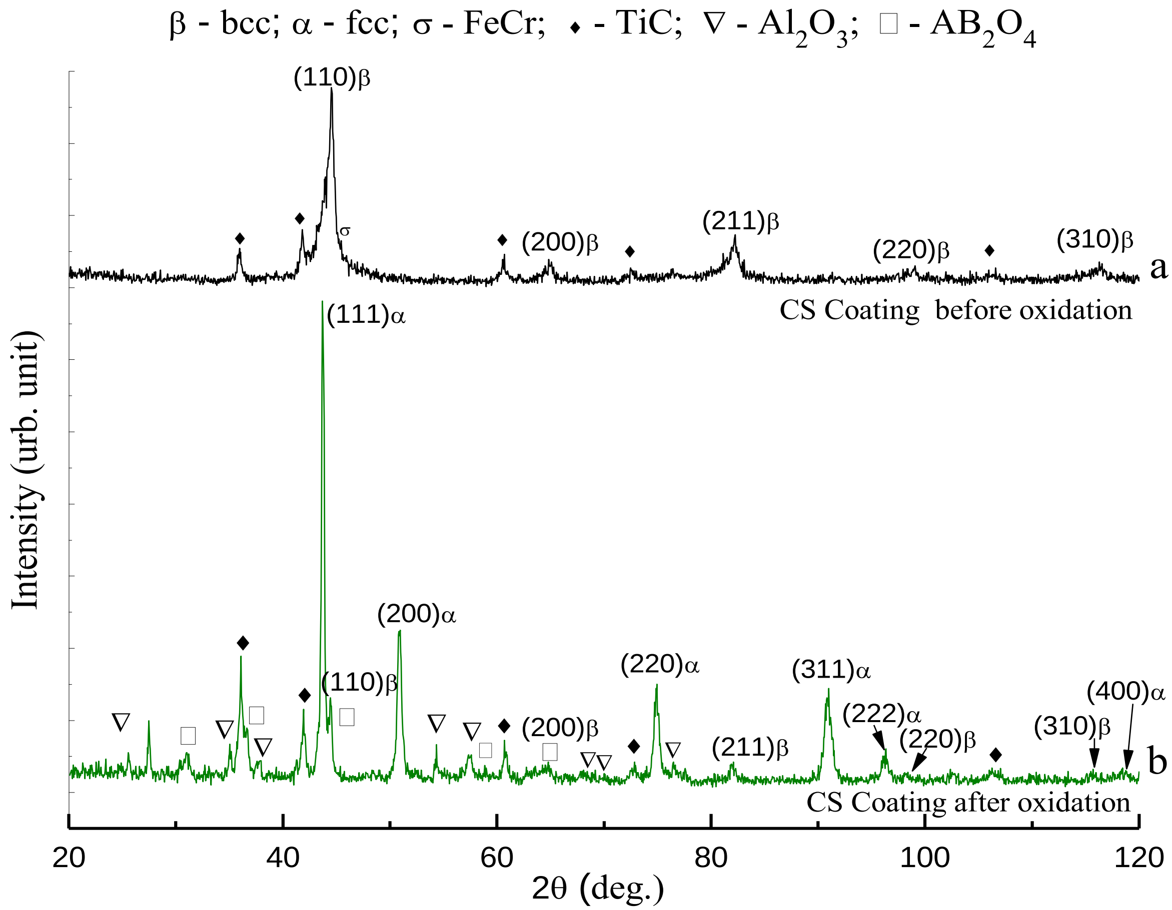

a – before oxidation, b – after oxidation

Figure 3.5 – XRD patterns of cold spray AlNiCoFeCrTi coatings on $Ni_{25}Cr$ substrate before and after oxidation at 900°C for 100 h

The results of X-ray phase analysis of the coating are confirmed by data obtained via BSE-SEM and spot EDX analysis. Fig. 3.6 a, b shows typical cross-sectional SEM images of AlNiCoFeCrTi high-entropy CS coating onto $Fe_{18}Cr$ steel substrate. In AlNiCoFeCrTi CS coating, a clear three-phase contrast is seen in BSE-SEM micrographs, as well as in SEM images of the feedstock powder on Fig. 3.2 b. While Fig. 3.6 c, d shows the cross-sectional SEM images of the coating after oxidation with Fig. 3.6 e, f shows the SEM images at the coating/substrate interface after oxidation. And also showing the results of the X-ray phase analysis of the coating on $Ni_{25}Cr$ substrate in Fig. 3.7.

The CS coating on $Fe_{18}Cr$ is relatively uniform, good interface between the coating and subtrate, it also thick. Having a mean thickness of about 400 μm which ranges due to the irregularity at the interface. In the coating / substrate interface, there are some small and large dark spots which are SiC particles that remained in the substrate surface after SiC blasting as shown in Fig 3.6 a, b. The CS coating on $Ni_{25}Cr$ substrate Fig. 3.7 a, b as a non-uniform coating thickness and rough coating surface, strong interaction between coating and substrate, showing also a dense coating, with a thickness of 130 μm which varies due to the roughness of the surface and interface, Also consist of the dark spots known to be SiC.

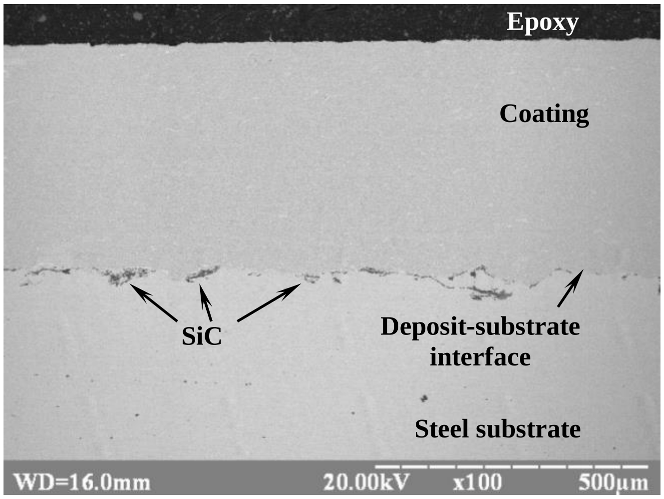

a

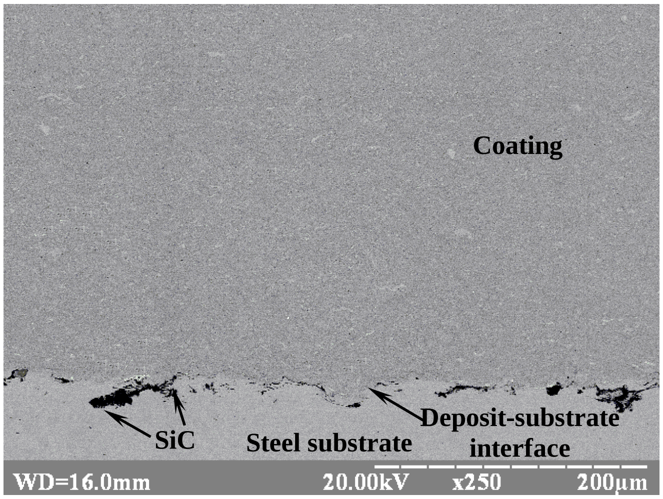

b

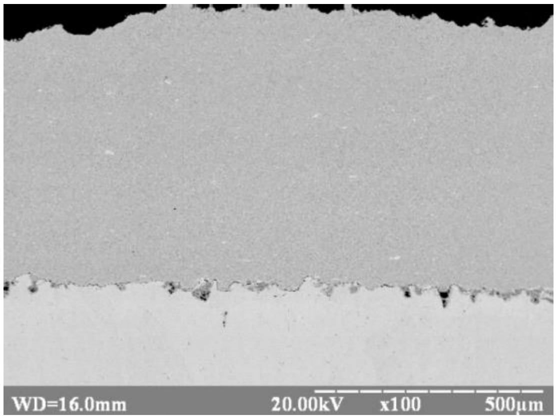

c

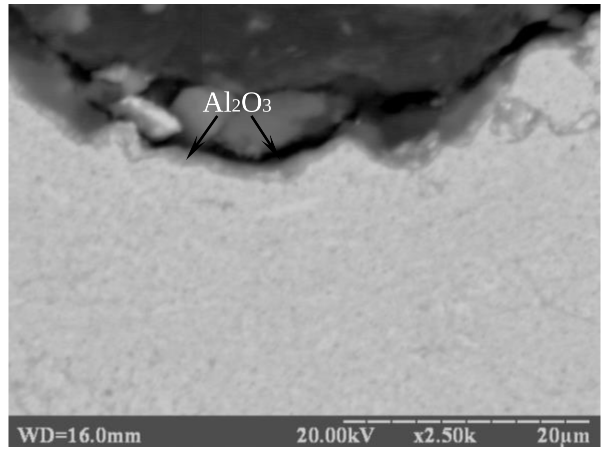

d

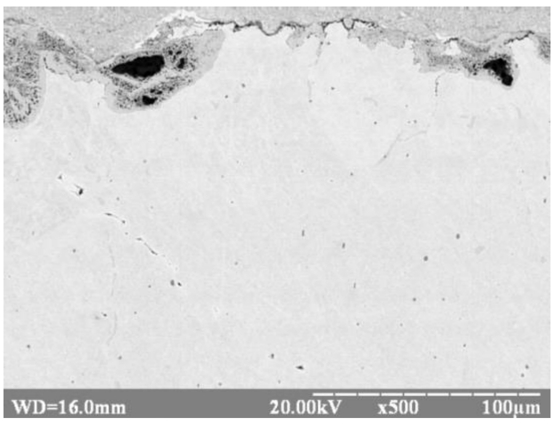

e

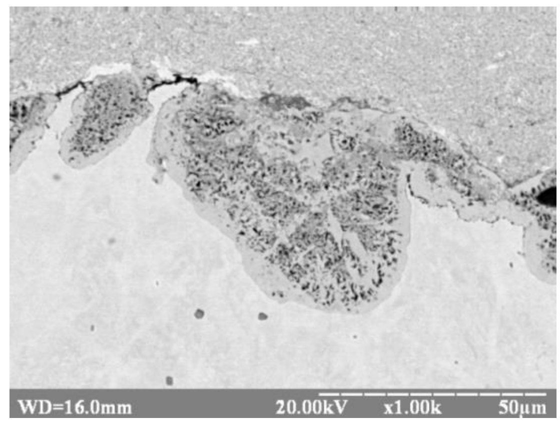

f

a, b – before oxidation (as-received); c, d – after oxidation; e, f – at the coating/substrate interface after oxidation

Figure 3.6 – SEM micrographs of cross-sectional microstructure of cold-sprayed AlNiCoFeCrTi coating on $Fe_{18}Cr$ substrate after oxidation at 900°C for 100 h

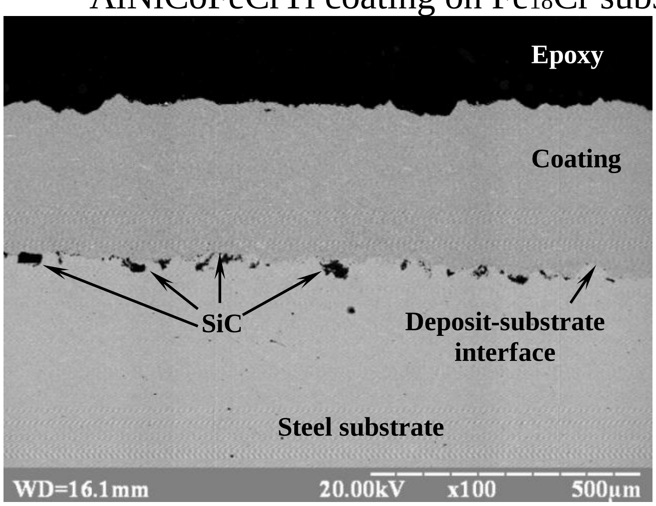

a

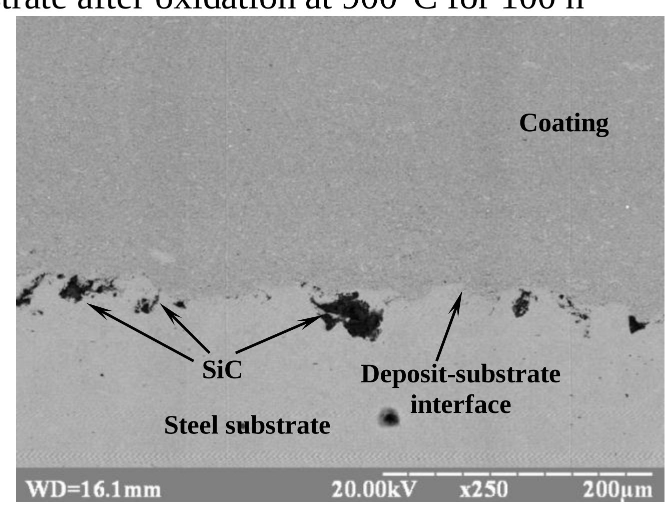

b

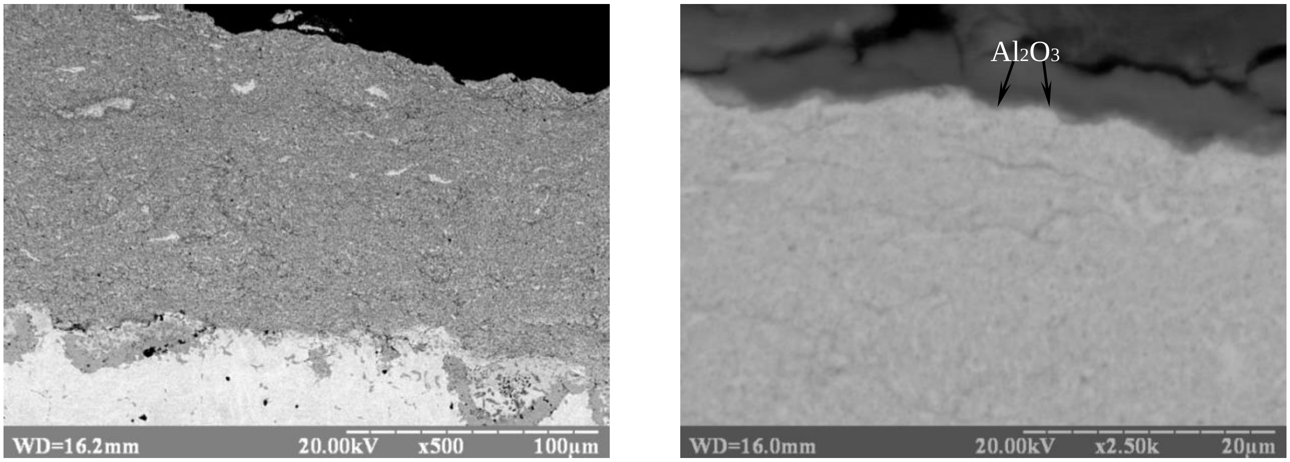

c d

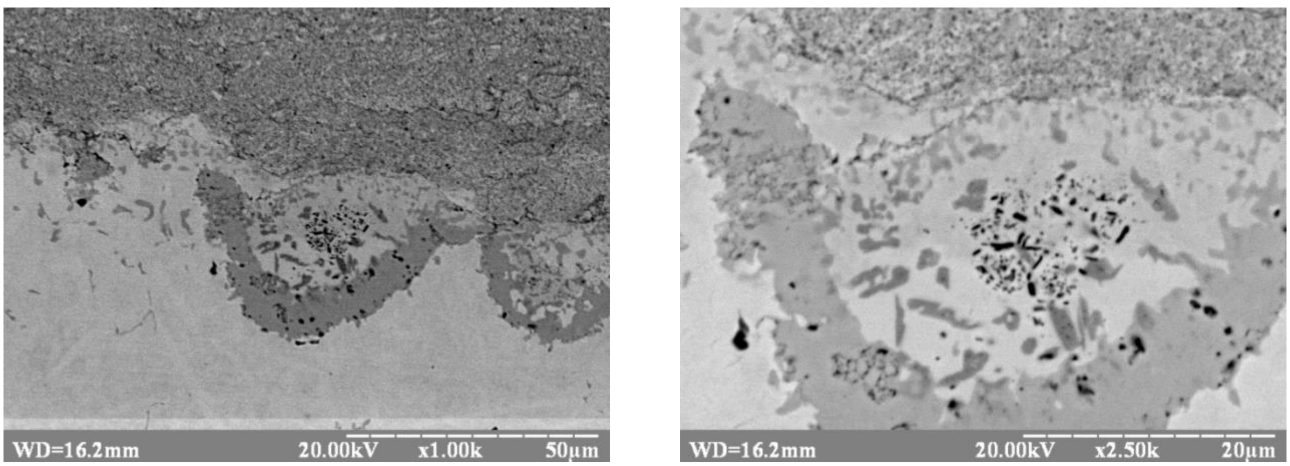

e f

a, b – before oxidation (as-received); c, d – after oxidation; e, f – at the coating/substrate interface after oxidation

Figure 3.7 – SEM micrographs of cross-sectional microstructure of cold-sprayed AlNiCoFeCrTi coating on $Ni_{25}Cr$ substrate after oxidation at 900 °C for 100 h.

3.3. Structure Characterization of AlNiCoFeCrTi High-Entropy Cold Spraying Coatings after oxidation

(XRD phase analysis (fig. 3.4b, 3.5 b), Cross-sectional SEM micrographs of the coating (fig. 3.6 c-f, 3.7 c-f),

Oxidation behaviour of cold spray AlNiCoFeCrTi HEA coating on Fe based substrate is shown in Fig. 3.4 b and 3.6 c-f.

Figure 3.4 b, Shows the XRD pattern taken at 900 ° C on the top surface of the coating after its oxidation. In the HEA literature it is well established that Al acts as a stabilizer for the BCC [94]. Alpha alumina and spinel peaks (type AB_2O_4), as seen in the figure, are evidence of this behaviour, while Al's simultaneous loss from the BCC process resulted in NiCoFeCrTi [94] an alloy of FCC below the oxide layer. It is also proved that Cr oxidizes to Cr_2O_3, which at temperatures above 1000 ° C volatilizes to CrO_3 [95]. Monitoring / capture of this process in such experiments is challenging, but this may influence the oxidation behavior of the HEA.

The characteristics observed based on close inspection of the oxidized samples shown in Fig. 3.6 c-f. cross-sectional BSE-SEM micrographs are as follows [96]:
(i) A thin layer of alumina is formed on the top of the CS coating, the remaining Al can be observed in the interphase dissolved in the alloy with particles of SiC seen in the SEM micrographs.
(ii) No oxide layer is formed at the interface of coating and substrate therefore no signs of porosity
(iii) the coating and the oxide layer appear to have sustained some damage during cross-sectional sample preparation.
The first promising conclusion from the above observations is that the current cold-sprayed AlCoCrFeNiTi coating oxidized to form an alumina layer which successfully protects the underlying substrate continuously from oxidation at 900° C for 100 h [96].

3.4 Microhardness of the AlNiCoFeCrTi High-Entropy Cold Spraying Coatings before and after oxidation

The Vickers microhardness of the CS coating on Fe based substrate was given to be 8.01 ± 0.4 GPa as shown in Fig. 3.8a the microhardness profile shows the microhardness to the distance of the surface of the coating and the subtrate which can be seen the high microhardness of the CS coating relative to the microhardness of the substrate The obvious strain hardening of the steel substrate resulting from the impact of extreme plastic deformation during the CS process can be noted. After oxidation at

900°C for 100h Fig. 3.8b the microhardness profile shows that the microhardness reduced to about 6.5 ± 0.4 GPa.

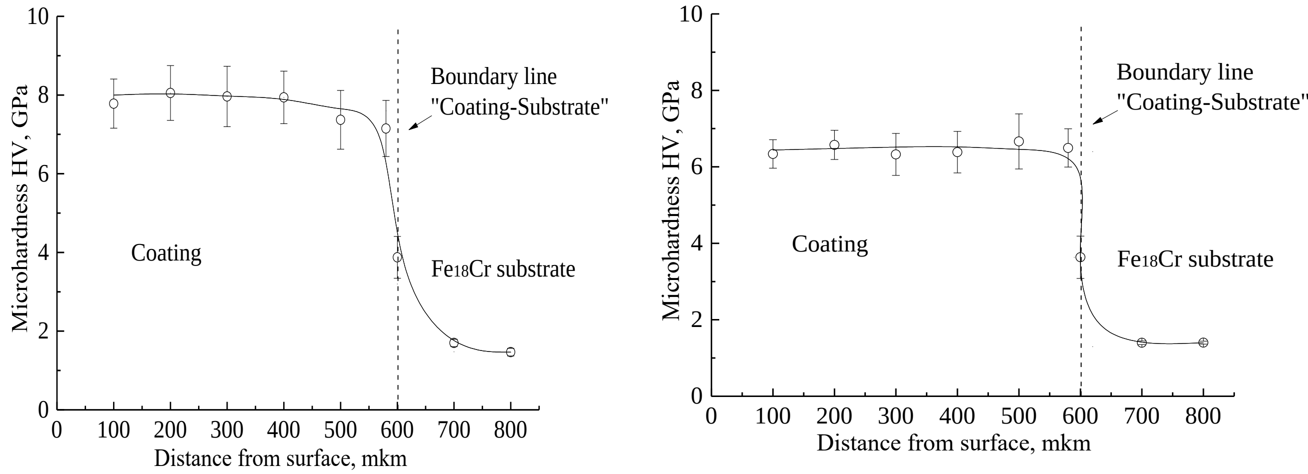

a b

Fig. 3.8 – Microhardness profile along the cross section of the CS AlNiCoFeCrTi coating on Fe based ($Fe_{18}Cr$) substrate: (a) before and (b) after oxidation at 900 °C for 100 h

Vickers microhardness of the CS coating on a nickel based substrate gave a relatively higher microhardness compared to the coasting on the Fe based substrate due to the less presence of the σ-phase (intermetallic FeCr compound) suggesting they are mostly dissolved into the AlNiCoFeCrTi high entropy alloy which was 8.71 ± 0.4 GPa. And after oxidation the result of the microhardness was said to be about 6.7 ± 0.4 GPa. The decrease in the microhardness of AlNiCoFeCrTi coatings after oxidation is caused by the influence of high temperature 900°C for a long time 100 hours. Under the prolonged influence of high temperature, phase and structural transformations occur, namely, a partial phase transformation of a stronger bcc solid solution to a less hard and more plastic fcc solid solution, dissolution of the intermetallic σ-phase in solid solutions, an increase in grain size / coherent-scattering region (CSR) and a decrease in the value of micro stresses due to recovery and recrystallization processes. The phase transformation under high temperature can be attributed to the metastable state of the supersaturated disordered bcc solid solution [97]. This metastable structure transforms during high temperature to more stable fcc and bcc solid solutions (α- and β phases). The XRD patterns in Fig. 3.4 and 3.5 show that heat treatment of the cold sprayed coatings at 900 °C for 100 hours results in their formation due to formation of metastable bcc phase during mechanical milling and CS which are a non-equilibrium processes.

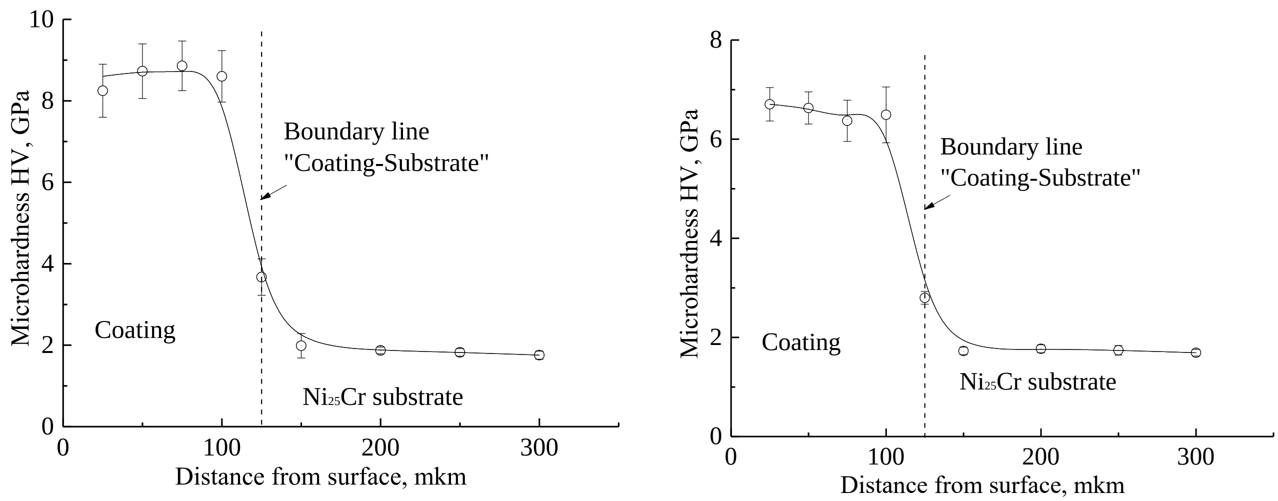

a b

Fig. 3.9 – Microhardness profile along the cross section of the CS AlNiCoFeCrTi coating on Ni based ($Ni_{25}Cr$) substrate: (a) before and (b) after oxidation at 900 °C for 100 h

CONCLUSIONS

In this work AlNiCoFeCrTi High entropy alloy coatings by cold spraying on steel, before and after oxidation were studied. These samples were characterized in the terms of their microstructure, phase composition, and various mechanical properties, which are required to provide extended lifetime of the component. The following findings can be summarized:

1. The important literature review shows that high entropy alloys (HEAs) due to their unique structure and properties are of great interest to the materials science and engineering community.
2. To manufacture AlNiCoFeCrTi HEA powder and to coat from it, the solid-state MA and CS technologies were applied respectively. It has been demonstrated that AlNiCoFeCrTi alloy nanocomposite powder formed by MA and annealing can be used as the feedstock for cold spray deposition of nanostructured HEA coatings on the steel substrates.
3. Cold spray is a feasible and potentially effective coating technique for producing HEA coatings while maintaining the coating's intrinsic alloy phases.
4. Equiatomic AlNiCoFeCrTi was successfully coated on substrates based on Fe and Ni. As-coating preserved the phases of MA.
5. Various characterization methods (Scanning Electron Microscope SEM, Ultima IV X-ray diffractometer XRD, Vickers microhardness machine PMT-3 were used to describe the morphology, microstructure, phase composition and microhardness of the feedstock powder and the coating.
6. AlNiCoFeCrTi coating formed a protective layer of alumina upon oxidation and was effective in preventing substrate oxidation for 100 h at 900 °C.

RECOMMENDATION

According to the results of microstructural (Fig. 3.1, 3.4, 3.5) and X-ray (Fig. 3.2, 3.3) studies:

– analyze the experimental data (Fig. 3.1, 3.2a, 3.3a) and determine the peculiarities of the morphology, structure and phase composition of the AlNiCoFeCrTi feed-stock powder for coating using cold gas dynamic deposition (CS);

– analyze the experimental data (Fig. 3.2b, 3.3b, 3.4, 3.5) and determine the peculiarities of the structure and phase composition of the AlNiCoFeCrTi CS coatings;

– determine the microhardness profile along the cross-section of the cold-sprayed AlNiCoFeCrTi coatings and substrates after oxidation;

– determine the microhardness changes in the AlNiCoFeCrTi coatings and substrates before (Figs. 3.6) and after oxidation.

Based on the obtained results, conclude on the effectiveness of CS method to obtain oxidation-resistant high-entropy coatings for potential applications at high operating temperatures.

HEA is an immense sector with endless new alloy systems. Our understanding of these new materials is still very preliminary and limited. As stated in this paper, our information focuses primarily on the Al-Ni-Co-Fe-Cr-Ti system, its derivatives and refractory HEAs- just a very small fraction of the entire HEA world. To better grasp the potentials of HEAs, further elements and combinations need to be explored. In order to achieve even greater strength, non-metallic elements such as C, B, and N may also be integrated.

With respect to HEAs phase and crystal structure. The equilibrium phases and phase diagrams are still little understood, but these are crucial to the design and development of HEAs. In this respect, significantly greater combination of experimental and computational research is required. Equimolar compositions are typically the simplest exposure to a new alloy framework, but they certainly do not possess the strongest combination of properties. Therefore, in those non-equimolar alloys, with precisely crafted composition and customized microstructures, there is potentially much more treasure. A successful approach is to start with equimolar alloys, and then extract from the equimolar alloy the desired non-equimolar composition [1].

REFERENCES

1. High-Entropy Alloys: A Critical Review. Materials Research / Tsai, Ming-Hung; Yeh, Jien-Wei // Letters. 30 April 2014. 2 (3): 107–123.

2. Atomic Structure Modeling of Multi-Principal-Element Alloys by the Principle of Maximum Entropy / Wang, Shaoqing (13 December 2013). V. **15** (12): 5536–5548.

3. High-Entropy Alloy: Challenges and prospects / Ye, YF; Wang, Q; Lu, J; Liu, CT; Yang, Y (July–August 2016 // Materials Today. **19** (6): 349–362.

4. Vincent AJB; Cantor B: part II thesis, University of Sussex (1981).

5**.** A study on multicomponent alloy systems containing equal-mole elements [M.S. thesis] / Huang KH, Yeh JW // Hsinchu: National Tsing Hua University; 1996.

6. https://www.mirror.co.uk/news/world-news/taiwanese-navy-accidentally-fires-nuclear-8730387

7. Nanostructured High-Entropy Alloys with Multiple Principal Elements: Novel Alloy Design Concepts and Outcomes / Yeh, J.-W.; Chen, S.-K.; Lin, S.-J.; Gan, J.-Y.; Chin, T.-S.; Shun, T.-T.; Tsau, C.-H.; Chang, S.-Y. (May 2004) // Advanced Engineering Materials. **6** (5): 299–303.

8. Microstructural development in equiatomic multicomponent alloys / Cantor, B.; Chang, I.T.H.; Knight, P.; Vincent, A.J.B. (July 2004). // Materials Science and Engineering: A. 375–377: 213–218.

9. Atomic scale modelling of hexagonal structured metallic fission product alloys / Middleburgh, S.C.; King, D.M.; Lumpkin, G.R. (April 2015). // . Royal Society Open Science. **2** (1): 140292.

10. Progress in Material Science / Y. Zhang et al., -V.61, P. 1-21 (2004).

11. High Entropy Alloy / Murty, B.S; Yeh, J.W; Ranganathan, S (2014). Pg 25

12. Introduction to the thermodynamics of materials / Gaskell DR. 3rd ed. Washinton (DC): Taylor & Francis; 1995.

13. Mechanical performance of the AlxCoCrCuFeNi high-entropy alloy system with multiprincipal elements / Tong CJ, Chen MR, Chen SK, Yeh JW, Shun TT, Lin SJ, Chang SY // Metall Mater Trans A. 2005;36:1263–1271.
14. Microstructure characterization of AlxCoCrCuFeNi high-entropy alloy system with multiprincipal elements / Tong CJ, Chen YL, Chen SK, Yeh JW, Shun TT, Tsau CH, Lin SJ, Chang SY // Metall Mater Trans A. 2005;36:881–893.
15. Thermodynamic analysis of the simple microstructure of AlCrFeNiCu high-entropy alloy with multi-principal elements / Li A, Zhang X. // Acta Metallurgica Sinica (English Letters). 2009;22:219–224.
16. Refractory high-entropy alloys. / Senkov ON, Wilks GB, Miracle DB, Chuang CP, Liaw PK. // Intermetallics. 2010;18:1758–1765.
17. Determination of the transition to the high entropy regime for alloys of refractory elements / Del Grosso MF, Bozzolo G, Mosca HO. // J Alloys Compd. 2012;534:25–31.
18. Entropy-driven phase stability and slow diffusion kinetics in an Al0.5CoCrCuFeNi high entropy alloy / Ng C, Guo S, Luan J, Shi S, Liu CT. // Intermetallics. 2012; 31:165–172.
19. Absence of long-range chemical ordering in equimolar FeCoCrNi. / Lucas MS, Wilks GB, Mauger L, Munoz JA, Senkov ON, Michel E, Horwath J, Semiatin SL, Stone MB, Abernathy DL, Karapetrova E. // Appl Phys Lett. 2012;100:251907.
20. Wear resistance and high-temperature compression strength of Fcc CuCoNiCrAl0.5Fe alloy with boron addition / Hsu CY, Yeh JW, Chen SK, Shun TT. // Metall Mater Trans A. 2004;35:1465–1469.
21. Effects of annealing treatment on phase composition and microstructure of CoCrFeNiTiAlx high-entropy alloys / Zhang KB, Fu ZY. // Intermetallics. 2012;22:24–32.
22 Relative effects of enthalpy and entropy on the phase stability of equiatomic high-entropy alloys / Otto F, Yang Y, Bei H, George EP. // Acta Mater. 2013;61:2628–2638.

23. Microstructure and aging behavior of Al5Cr32Fe35Ni22Ti6 ternary-like high-entropy alloy. / Lin CW, Tsai MH, Tsai CW, Yeh JW, Chen SK. In preparation.
24. Recent progress in multi-element alloy and nitride coatings sputtered from high-entropy alloy targets / Cheng KH, Lai CH, Lin SJ, Yeh JW. // Ann Chim-Sci Mat. 2006;31:723–736.
25. Sluggish diffusion in Co–Cr–Fe–Mn–Ni high-entropy alloys / Tsai KY, Tsai MH, Yeh JW. // Acta Mater. 2013;61:4887–4897.
26 Corrosion properties of a novel bulk Cu0.5NiAlCoCrFeSi glassy alloy in 288◦C high-purity water / Chen YY, Duval T, Hong UT, Yeh JW, Shih HC, Wang LH, Oung JC. // Mater Lett. 2007;61:2692–2696.
27 Decomposition in multi-component AlCoCrCuFeNi high-entropy alloy / Singh S, Wanderka N, Murty BS, Glatzel U, Ban-hart J. // Acta Mater. 2011;59:182–190.
28. Diffusion barrier properties of AlMoNbSiTaTiVZr high-entropy alloy layerbbetween copper and silicon / Tsai MH, Yeh JW, Gan JY. // Thin Solid Films. 2008;516:5527–5530.
29. Thermal stability and performance of NbSiTaTiZr high-entropy alloy barrier for copper metallization / Tsai MH, Wang CW, Tsai CW, Shen WJ, Yeh JW, Gan JY, Wu WW. // J Electrochem Soc. 2011;158:1161–1165.
30. Physical properties of high entropy alloys/ Tsai MH. // Entropy. 2013;15:5338–5345.
31. Anomalous Decrease in X-ray Diffraction Intensities of CuNiAlCoCrFeSi Alloy Systems with Multi-principal Elements / J.W. Yeh, S.Y. Chang, Y.D. Hong and et. al. – Hsinchu : Materials Chemistry and Physics, 2007.
32. Structure of intermetallic compounds and phases / Ferro P, Saccone A. In: Cahn RW, Haasen P. // Physical metallurgy. 4th ed.Amsterdam, the Netherlands: Elsevier Science B.V.; 1996
33. Confusion by design / Greer, A. Lindsay // (25 December 1993) Nature. **366** (6453): 303–304.

34. Zhang, Y.; Zhou, Y. J.; Lin, J. P.; Chen, G. L.; Liaw, P. K. Solid-Solution Phase Formation Rules for Multi-component Alloys // Advanced Engineering Materials. (June 2008) **10** (6): 534–538.

35. Takeuchi, Akira; Inoue, Akihisa (2005). "Classification of Bulk Metallic Glasses by Atomic Size Difference, Heat of Mixing and Period of Constituent Elements and Its Application to Characterization of the Main Alloying Element". Materials Transactions. **46** (12): 2817–2829.

36. Otto, F.; Yang, Y.; Bei, H.; George, E.P. (April 2013). "Relative effects of enthalpy and entropy on the phase stability of equiatomic high-entropy alloys". Acta Materialia. **61** (7): 2628–2638.

37. Zhang, Yong; Zuo, Ting Ting; Tang, Zhi; Gao, Michael C.; Dahmen, Karin A.; Liaw, Peter K.; Lu, Zhao Ping (April 2014). "Microstructures and properties of high-entropy alloys". Progress in Materials Science. **61**: 1–93.

38. Cahn RW, Haasen P., editors Physical metallurgy. 4th ed.Amsterdam, the Netherlands: Elsevier Science B.V.; 1996

39. Guo S, Liu CT. Phase stability in high entropy alloys: formation of solid-solution phase or amorphous phase. Prog Nat Sci: Mater Int. 2011;21:433–446.

40. https://en.wikipedia.org/wiki/Gibbs_free_energy

41. Guo S, Ng C, Lu J, Liu CT. Effect of valence electron concentration on stability of fcc or bcc phase in high entropy alloys. J Appl Phys. 2011;109:103505. doi: 10.1063/1.3587228

42. Otto, F.; Dlouhý, A.; Somsen, Ch.; Bei, H.; Eggeler, G.; George, E.P. (September 2013). "The influences of temperature and microstructure on the tensile properties of a CoCrFeMnNi high-entropy alloy". Acta Materialia. **61** (15): 5743–5755.

43. Wu, Z.; Bei, H.; Otto, F.; Pharr, G.M.; George, E.P. (March 2014). "Recovery, recrystallization, grain growth and phase stability of a family of FCC-structured multi-component equiatomic solid solution alloys". Intermetallics. **46**:131–140.

44. Zaddach, A.J.; Scattergood, R.O.; Koch, C.C. (June 2015). "Tensile properties of low-stacking fault energy high-entropy alloys". Materials Science and Engineering: A. **636**: 373–378.
45. Hemphill, M.A.; Yuan, T.; Wang, G.Y.; Yeh, J.W.; Tsai, C.W.; Chuang, A.; Liaw, P.K. (September 2012). "Fatigue behavior of Al0.5CoCrCuFeNi high-entropy alloys". Acta Materialia. **60** (16): 5723–5734.
46. Youssef, Khaled M.; Zaddach, Alexander J.; Niu, Changning; Irving, Douglas L.; Koch, Carl C. (9 December 2014). "A Novel Low-Density, High-Hardness, High-entropy Alloy with Close-packed Single-phase Nanocrystalline Structures". Materials Research Letters. **3** (2): 95–99.
47. Shipman, Matt. "New 'high-entropy' alloy is as light as aluminum, as strong as titanium alloys". Phys.org. Retrieved 29 May 2015.
48. Zou, Yu; Ma, Huan; Spolenak, Ralph (2015-07-10). "Ultrastrong ductile and stable high-entropy alloys at small scales". Nature Communications. **6**: 7748.
49. Zou, Yu; Maiti, Soumyadipta; Steurer, Walter; Spolenak, Ralph (2014-02-15). "Size-dependent plasticity in an Nb25Mo25Ta25W25 refractory high-entropy alloy". Acta Materialia. **65**: 85–97.
50. https://phys.org/news/2018-11-strength-ductility-high-entropy-alloy-oxygen.html
51. Chuang MH, Tsai MH, Wang WR, Lin SJ, Yeh JW. Microstructure and wear behavior of $Alj_xCo_{1.5}CrFeNi_{1.5}Ti_y$ high-entropy alloys. Acta Mater. 2011;59: 6308–6317.
52. Chen ST, Tang WY, Kuo YF, Chen SY, Tsau CH, Shun TT, Yeh JW.
Microstructure and properties of age-hardenable $Alj_xCrFe_{1.5}MnNi_{0.5}$ alloys. Mater Sci Eng A. 2010;527:5818–5825.
53. Lin CM, Tsai HL. Evolution of microstructure, hardness, and corrosion properties of high-entropy $Al_{0.5}CoCrFeNi$ alloy. Intermetallics. 2011;19:288–294

54. Chen YY, Duval T, Hung UD, Yeh JW, Shih HC. Microstructure and electrochemical properties of high entropy alloys—a comparison with type-304 stainless steel. Corros Sci. 2005;47:2257–2279.

55. Hsu YJ, Chiang WC, Wu JK. Corrosion behavior of $FeCoNiCrCuj_{x}$ high-entropy alloys in 3.5% sodium chloride solution. Mater Chem Phys. 2005;92:112–117.

56. Lin CM, Tsai HL, Bor HY. Effect of aging treatment on microstructure and properties of high-entropy $Cu_{0.5}CoCrFeNi$ alloy. Intermetallics. 2010;18: 1244–1250.

57. Lee CP, Chang CC, Chen YY, Yeh JW, Shih HC. Effect of the aluminium content of $Alj_{x}CrFe_{1.5}MnNi_{0.5}$ high-entropy alloys on. the corrosion behaviour in aqueous environments. Corros Sci. 2008;50:2053–2060.

58. Chou YL, Wang YC, Yeh JW, Shih HC. Pitting corrosion of the high-entropy alloy $Co_{1.5}CrFeNi_{1.5}Ti_{0.5}Mo_{0.1}$ in chloride-containing sulphate solutions. Corros Sci. 2010;52:3481–3491

59. Chou YL, Yeh JW, Shih HC. Effect of molybdenum on the pitting resistance of $Co_{1.5}CrFeNi_{1.5}Ti_{0.5}Moj_{x}$ alloys in chloride solutions. Corrosion. 2011;67:085002.

60. Chou YL, Yeh JW, Shih HC. The effect of molybdenum on the corrosion behaviour of the high-entropy alloys $Co_{1.5}CrFeNi_{1.5}Ti_{0.5}Moj_{x}$ in aqueous environments. Corros Sci. 2010;52:2571–2581

61. Kao YF, Lee TD, Chen SK, Chang YS. Electrochemical passive properties of $Alj_{x}CoCrFeNi$ (x=0, 0.25, 0.50, 1.00) alloys in sulfuric acids. Corros Sci. 2010;52: 1026–1034.

62. Lee CP, Chen YY, Hsu CY, Yeh JW, Shih HC. The effect of boron on the corrosion resistance of the high entropy alloys $Al_{0.5}CoCrCuFeNiB_{x}$. J Electrochem Soc. 2007;154:C424–C430.

63. Wang YP, Li BS, Ren MX, Yang C, Fu HZ. Microstructure and compressive properties of AlCrFeCoNi high entropy alloy. Mater Sci Eng A. 2008;491: 154–158.

64. Murty, B.S; Yeh, J.W; Ranganathan, S (2014). “High Entropy Alloy”. structure properties Pg 146-148

65. Murty, B.S; Yeh, J.W; Ranganathan, S (2014). “High Entropy Alloy”. structure properties Pg 157.
66. Granberg, Fredric (2016). "Mechanism of radiation damage reduction in equiatomic multicomponent single phase alloys". Physical Review Letters. **116** (13): 135504.
67. Jansson, Ulf; Claudia Zlotea; Karlsson, Dennis; Sahlberg, Martin (2016-11-10). "Superior hydrogen storage in high entropy alloys". Scientific Reports. **6**: 36770.
68. Karlsson, Dennis; Ek, Gustav; Cedervall, Johan; Zlotea, Claudia; Møller, Kasper Trans; Hansen, Thomas Christian; Bednarčík, Jozef; Paskevicius, Mark; Sørby, Magnus Helgerud (2018-02-19). "Structure and Hydrogenation Properties of a HfNbTiVZr High-Entropy Alloy". Inorganic Chemistry. **57** (4): 2103–2110.
69. Michael C. Gao; Jien-Wei Yeh; Peter K. Liaw ; Yong Zhang, (2016) (1)516 High-entropy alloys: Fundamentals and applications
70. Varalakshmi S. Synthesis and characterization of nanocrystalline high entropy alloys by mechanical alloying. Ph.D. Thesis, Department of Metallurgical and Materials Engineering, Indian Institute of Technology, Madras, 2008.
71. Chen YL, Hu YH, Tsai CW, Hsieh CA, Kao SW, Yeh JW, Chin TS, Chen SK Alloying behavior of binary to octonary alloys based on Cu–Ni–Al–Co–Cr–Fe–Ti–Mo during mechanical alloying. J Alloys Compd. – 2009. – V. 477 (1–2). –P. 696–705.
72. Zhang KB, Fu ZY, Zhang JY, Shi J, Wang WM, Wang H, Wang YC, Zhang Q.J. Nanocrystalline CoCrFeNiCuAl high-entropy solid solution synthesized by mechanical alloying. J Alloys Compd. – 2009. – Мю 485(1–2)ю – P. L31–L34.
73. Praveen S, Murty BS, Kottada RS (2012) Alloying behavior in multi-component AlCoCrCuFeand high entropy alloys. Mater Sci Eng A 534:83–89.
74. http://en.wikipedia.org/wiki/Cladding_%28metalworking%29
75. Schnell A, Kurz W Epitaxial deposition of MCrAlY coatings on a Ni-base superalloyby laser cladding. Scr. Mater. 2003, 49(7):705–709.
76. http://en.wikipedia.org/wiki/Sputter_deposition
77.http://groups.ist.utl.pt/rschwarz/rschwarzgroup_files/PLD_files/PLD.htm

78. https://en.wikipedia.org/wiki/Thermal_spraying
79. Kuroda, Seiji; Kawakita, Jin; Watanabe, Makoto; Katanoda, Hiroshi. "Warm spraying—a novel coating process based on high-velocity impact of solid particles". Sci. Technol. Adv. Mater. 2008, **9** (3): 033002
80. Moridi, A.; Hassani-Gangaraj, S. M.; Guagliano, M.; Dao, M. "Cold spray coating: review of material systems and future perspectives". Surface Engineering. 2014. **30** (6): 369–395.
81. Boer, F.R. de, Mattens, W.C.M., Boom, R., Miedema, A.R., & Niessen, A.K. (1988). Cohesion in metals. Netherlands: North-Holland.
82. A.P.Alkhimov, V.F. Kosarev, N.I. Nesterovich, A.N. Papyrin., Method of applying coatings (SU1618778), 1980.
83. A.P. Alkhimov, V.F. Kosareve, A.N. Papyrin, A Method of Cold Gas-Dynamic Spray Deposition, Dokl.
84. H. Assadi, H. Kreye, F. Gärtner, T. Klassen, Cold spraying – A materials perspective, Acta Mater. 116 (2016) 382–407.
85. R.N. Raoelison, Y. Xie, T. Sapanathan, M.P. Planche, R. Kromer, S. Costil, et al., Cold gas dynamic spray technology: A comprehensive review of processing conditions for various technological developments till to date, Addit. Manuf. 19 (2018) 134–159.
86. M.R. Rokni, S.R. Nutt, C.A. Widener, V.K. Champagne, R.H. Hrabe, Review of Relationship Between Particle Deformation, Coating Microstructure, and Properties in High-Pressure Cold Spray, J. Therm. Spray Technol. (2017) 1–48.
87. M. Hassani-Gangaraj, D. Veysset, K.A. Nelson, C. Schuh, In-situ observations of single micro-particle impact bonding, Scr. Mater. in press (2017) 9–13.
88. F. Meng, S. Yue, J. Song, Quantitative prediction of critical velocity and deposition efficiency in cold- spray: A finite-element study, Scr. Mater. 107 (2015) 83–87.
89. H. Assadi, F. Gärtner, T. Stoltenhoff, H. Kreye, Bonding mechanism in cold gas spraying, Acta Mater. 51 (2003) 4379–4394.

90. F.F. Raletz, M. Vardelle, G. Ezo'o, Critical particle velocity under cold spray conditions, Surf. Coatings Technol. (2006), V. 201, P. 1942–1947.

91. M. Hassani-Gangaraj, D. Veysset, K.A. Nelson, C.A. Schuh, Melting can hinder impact-induced adhesion, Phys. Rev. Lett. 2017, 1–5.

92. Effect of temperature on mechanical properties of Al0.5CoCrCuFeNi wrought alloy / Tsai CW, Tsai MH, Yeh JW, Yang CC // J Alloys Compd. 2010;490:160–165.

93. Hushchyk, D.V., Yurkova, A.I., Cherniavsky, V.V. et al. Nanostructured AlNiCoFeCrTi high-entropy coating performed by cold spray. Appl Nanosci (2020).

94. W-R. Wang, W-L. Wang, S-C. Wang, Y-C. Tsai, C-H. Lai, and J-W. Yeh: Effects of Al addition on the microstructure andmechanical property of AlxCoCrFeNi high-entropy alloys.Intermetallics 26, 44 (2012)

95. C.S. Tedmon, Jr.: The effect of oxide volatilization on the oxidation kinetics of Cr and Fe–Cr alloys. J. Electrochem. Soc. 113,766 (1966).

96. Anupam, Ameey & Kumar, S. & Chavan, Naveen & Murty, Budaraju & Kottada, Ravi Sankar. (2019). First report on cold-sprayed AlCoCrFeNi high-entropy alloy and its isothermal oxidation. Journal of Materials Research. 34. 1-11.

97. Yurkova A.I, Cherniavsky V.V, Bolbut V., Krüger M., Bogomol I. (2019). Structure formation and mechanical properties of the highentropy AlCuNiFeCr alloy prepared by mechanical alloying and spark plasma sintering. J Alloy Compd 786:139–148.